

www.acsami.org Spotlight on Applications

Charged Particle-Induced Surface Reactions of Organometallic Complexes as a Guide to Precursor Design for Electron- and Ion-Induced Deposition of Nanostructures

Jo-Chi Yu, Mohammed K. Abdel-Rahman, D. Howard Fairbrother, and Lisa McElwee-White*



Cite This: ACS Appl. Mater. Interfaces 2021, 13, 48333–48348

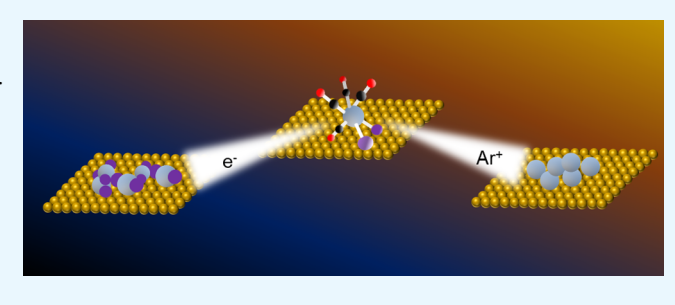


ACCESS

III Metrics & More

Article Recommendations

ABSTRACT: Focused electron beam-induced deposition (FEBID) and focused ion beam-induced deposition (FIBID) are direct-write fabrication techniques that use focused beams of charged particles (electrons or ions) to create 3D metal-containing nanostructures by decomposing organometallic precursors onto substrates in a low-pressure environment. For many applications, it is important to minimize contamination of these nanostructures by impurities from incomplete ligand dissociation and desorption. This spotlight on applications describes the use of ultra high vacuum surface science studies to obtain mechanistic information



on electron- and ion-induced processes in organometallic precursor candidates. The results are used for the mechanism-based design of custom precursors for FEBID and FIBID.

KEYWORDS: electron beam-induced deposition, FEBID, ion beam-induced deposition, FIBID, precursor chemistry, charged particle-induced deposition, 3D nanostructure fabrication

■ INTRODUCTION

Focused electron beam-induced deposition (FEBID) (Figure 1) and focused ion beam-induced deposition (FIBID) are powerful nanofabrication techniques that utilize charged particles to drive deposition of spatially and geometrically well-defined 3D nanostructures from precursor compounds. 1 FEBID and FIBID are direct-write lithographic processes that can generate metal-containing nanostructures with precise control on planar and nonplanar surfaces without the need for masks or resists. As a result, FEBID has been used for industrial applications such as circuit editing⁵ and photomask repair.⁶⁻⁹ FEBID using ruthenium precursors has also been suggested for use in fabricating and repairing the capping layer of photomasks for extreme ultraviolet lithography (EUVL) 10,11 This deposition technique is also applied in academic research such as fabricating tips for local probe microscopes 12,13 producing nanophotonic and nanoplasmonic structures. 14-16 FIBID has been used industrially in the repair of photomasks for both standard lithography (the Aerial Image Measurement System (AIMS) for 193 nm lithography)9 and EUVL17 and in TEM lamella preparation¹⁸ and circuit editing. 19

FEBID is typically conducted in electron microscopes, with a background pressure of 1×10^{-7} to 1×10^{-5} Torr during delivery of a constant flux of volatile precursors. Precursor compounds adsorb to the substrate surface and are then exposed to a high energy (>500 eV) primary electron beam (Figure 1). The interaction of the primary electrons with the

substrate creates secondary electrons that undergo scattering as illustrated in Figure 2a. These lower energy (0-100 eV) secondary electrons initiate precursor dissociation. Volatile species generated in this process desorb from the substrate, leaving behind a nonvolatile deposit that includes metal atoms and unwanted organic contamination.

The ion beam deposition technique FIBID³ has higher current density, a shorter penetration path in a solid substrate, and a wider choice of charged particle sources when compared to the electron beam used in FEBID.²⁰ In contrast to FEBID, precursor decomposition in FIBID is less well understood and may involve contributions from the low energy secondary electrons generated by exposure to the ion beam but also effects due to collisions between ions and adsorbed precursor molecules and localized temperature spikes that result from energy dissipation in the solid.³ Moreover, in FIBID (Figure 2b),³ surface sputtering operates in parallel with deposition. This concomitant sputtering has the benefit of serving as a purification method to remove unwanted contaminants that

Received: July 8, 2021 Accepted: September 24, 2021 Published: October 11, 2021





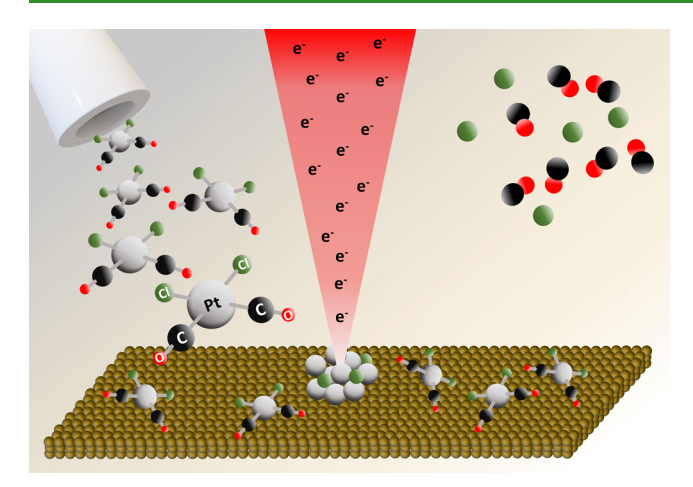


Figure 1. An illustration of FEBID from Pt(CO)₂Cl₂ as precursor. The Pt(CO)₂Cl₂ molecules are introduced via gas injection system (GIS) and physisorb onto the substrate. The focused electron beam interacts with the physisorbed molecules and stimulates precursor decomposition. The volatile fragments (CO and Cl⁻) are mostly desorbed under vacuum conditions, whereas the nonvolatile components (Pt and some Cl atoms) form a deposit.

derive from precursor ligands, but it also partially etches away the metal atoms in the deposit. To produce a high metal content deposit with a reasonable thickness, finding the balance between sputtering and deposition is therefore crucial. Potential problems with FIBID include overetching, amorphization, and ion implantation.²¹ Because of the possibility of ion implantation during deposition, the ion source has been of interest in the development of FIBID. Problems with contamination from Ga⁺ ion beams³ have led to significant efforts toward developing alternative gas field ion sources (GFISs), e.g., He⁺, Ne⁺, and Ar⁺. With the smaller probe sizes of these GFISs, it became possible for FIBID to produce three-dimensional structures in the subnanometer range with lower damage and no additional contamination in the deposit.^{22,23}

■ PRECURSOR DESIGN FOR FEBID/FIBID

Precursor requirements for FEBID/FIBID^{24–26} share some features with the properties required for other deposition techniques that utilize gas phase delivery, such as chemical vapor deposition (CVD)²⁷ and atomic layer deposition (ALD).^{28,29} For all of these techniques, precursors for practical use must be readily available, stable during storage and

handling, volatile enough for transport to the substrate surface, and thermally stable enough to survive the volatilization and gas phase transport processes. Most importantly, precursors must undergo decomposition to the desired product under the deposition conditions. However, differences in the decomposition mechanisms between thermal processes such as CVD/ALD and charged particle-induced processes such as FEBID/FIBID have led to the need for development of custom precursors for FEBID/FIBID.

One of the main challenges for FEBID and FIBID is to minimize contamination derived from ligand decomposition in the deposited material. Mechanism-based precursor design^{24–26} uses modeling and understanding of the decomposition processes to identify potential ligands for organometallic precursors. The goal of the model studies is to identify ligands or groups of ligands that desorb cleanly during the deposition process upon bombardment by ions or irradiation by electrons.³⁰

After identification of appropriate ligands for precursors, candidate complexes can be chosen by consideration of their oxidation state and coordination sphere to minimize the chances of ligand-derived contamination. As an example, in considering Pt precursors, the commonly available oxidation states are Pt(0), Pt(II), and Pt(IV). For the lower oxidation states Pt(0) and Pt(II), four-coordinate complexes are most common.31 To achieve the preferred 16 e square planar complexes of Pt(0), the common formula is PtL4 with four neutral ligands L, whereas Pt(II) complexes are generally of the type PtL₂X₂ with two neutral ligands L and two negatively charged ligands X. In contrast, the higher valent Pt(IV) compounds tend to be six-coordinate. Using a strategy of minimizing contamination from ligand fragments by minimizing the number of ligand atoms in the precursor, fourcoordinate Pt(0) or Pt(II) complexes would be more likely to be suitable as precursor candidates for FEBID/FIBID than the six-coordinate Pt(IV) compounds.³¹ This strategy has been validated in studies of Pt precursors (vide infra).

Sufficient volatility for precursor evaporation and transport in the GIS is also critical. Molecular weight is a consideration, as mononuclear complexes tend to (but do not always) have higher vapor pressures than binuclear complexes and clusters. There are also known relationships between intermolecular interactions and volatility. For example, complexes that are capable of hydrogen bonding generally have low vapor pressures.³³ Complexes with fluorinated ligands are more

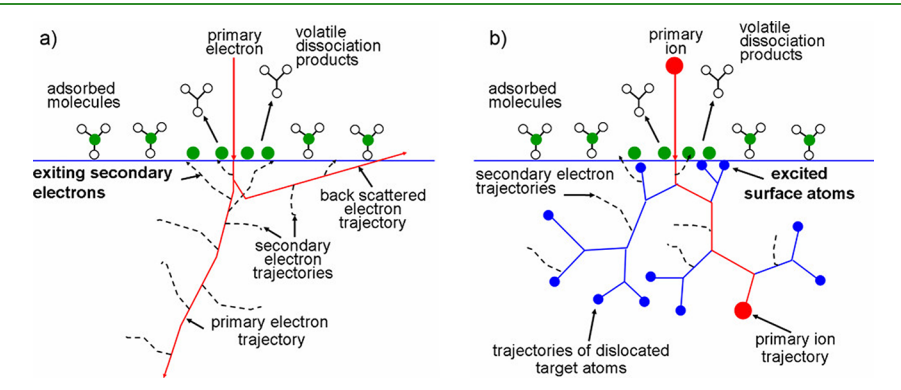


Figure 2. (a) Scheme of interactions of primary electrons generating an emitted flux of secondary electrons and backscattered electrons. All electrons can dissociate surface adsorbed molecules via electronic excitation. (b) Scheme of interactions of primary ions generating secondary electrons and a collision cascade of substrate atoms.³ Reproduced with permission from ref 3. Copyright 2008 American Vacuum Society.

volatile than their hydrocarbon analogues because of repulsion between the fluorine lone pairs.³⁴ For solid precursors, assessing the intermolecular interactions in the solid state by analysis of single-crystal X-ray structures has been an effective means of identifying complexes with lower sublimation temperatures.³⁵ These strategies provide guidance for initial choice of precursor candidates; however, experimental determination of conditions for sublimation and transport by sublimation under carefully controlled pressures³⁵ and measurement of sublimation and decomposition temperatures by thermogravimetric analysis³⁶ remain the best means of assessment of volatility.

MODELING FEBID/FIBID WITH ULTRAHIGH VACUUM (UHV) SURFACE SCIENCE STUDIES

The mechanism-based design of custom precursors for charged particle-induced techniques, such as FEBID and FIBID, requires a means of elucidating the reactions of candidate complexes under electron- or ion-beam irradiation. Ultrahigh vacuum (UHV) surface science studies (Figure 3) can be used

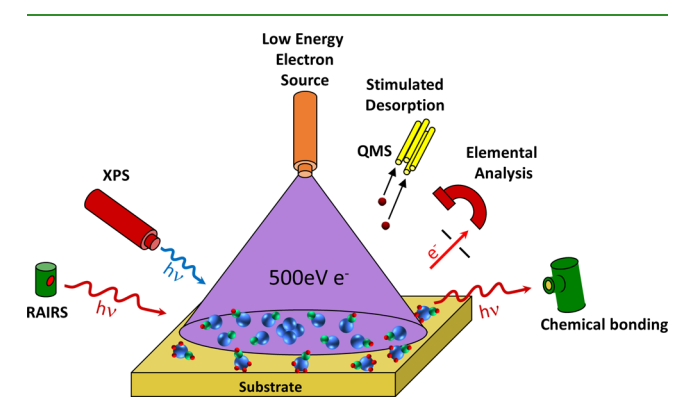


Figure 3. Schematic representation of the ultrahigh vacuum surface science approach to studying FEBID precursors.

to model FEBID/FIBID and provide insight into the mechanistic details of precursor decomposition upon irradiation with low energy secondary electrons or ions. In this approach, precursor molecules physisorb from the gas phase onto a cold substrate (<200 K) to form a 1-2 monolayer (ML) film under UHV ($<5 \times 10^{-9}$ Torr). The substrates were chosen to be inert and to not have any spectral interference with XPS peaks from the precursor. Gold was used as the substrate in almost all cases, although on occasion other substrates such as HOPG or oxidized silicon were used. Although we have never explicitly studied the effect of precursor surface coverage, we have generally observed no substantive differences in the reactions we observe when we compare between different film thicknesses. This would lead us to conclude that there are no strong coverage effects, at least in the monolayer coverage regime we are typically working in, and that the reactions are principally a consequence of the interactions between the charged particles and individual adsorbate (precursor) molecules.

After exposure to electrons from a flood gun or ions from an ion gun, the resulting material can be characterized using standard surface spectroscopic techniques such as X-ray photoelectron spectroscopy (XPS), while volatile fragments that desorb during the deposition process can be probed by mass spectrometry. There are three main differences between

FEBID/FIBID and UHV conditions. First, the higher vacuum of UHV provides a cleaner environment, in contrast to the HV environment of an SEM chamber, where impurities (e.g., hydrocarbons, water vapor) in the chamber background can introduce impurities during deposition. Second, the electron or ion source in UHV modeling creates a diffuse beam of electrons or ions on the same scale as the sample dimensions (typically ~1 cm²) suitable for XPS analysis. In the case of FEBID, the energy of the primary electrons generated by the flood gun (500 eV) is sufficient to generate low energy secondary electrons, which are considered responsible for the electron-induced molecular decomposition in FEBID. 37-39 Third, the low temperatures required to prevent the physisorbed precursor molecules from desorbing in UHV can preclude thermal decomposition steps involved in the overall deposition process at the near room temperature substrate temperatures prevalent in conventional FEBID/FIBID. However, the limitation of these low temperatures can be addressed to a degree by probing the effect of annealing films initially exposed to electrons or ions to room temperature. Despite the differences in experimental conditions between the UHV surface science studies and FEBID/FIBID, they remain an effective means of providing mechanistic information on charged particle-induced precursor decomposition.

By studying the decomposition behavior of metal complexes with various types of ligands, we have identified privileged ligands, such as CO, that cleanly desorb under FEBID/FIBID conditions. ^{24,25} In this review, we present case studies of using UHV surface science experiments to evaluate precursors for deposition of Pt, Ru, Au, and alloy structures by FEBID/FIBID. The structures of the precursor complexes are shown in Chart 1. Gas phase studies describing the reactions of precursors with electrons ^{40–44} and ions ⁴⁵ have provided a useful set of information that is complementary to the data from surface studies but those experiments are outside the scope of this spotlight.

■ DEPOSITION OF PT BY FEBID AND FIBID

Platinum nanostructures have applications in electronic devices, \$^{46,47}\$ sensors, \$^{48,49}\$ and catalysts. \$^{50-53}\$ FEBID and FIBID allow for controlled fabrication of metal nanostructures with subnanometer spatial resolution. \$^{54}\$ In general, FEBID studies have targeted means to fabricate highly pure metal deposits. However, deposits composed of Pt nanocrystals embedded in amorphous carbon that are typical of FEBID from organometallic precursors \$^{55}\$ may also have practical applications. \$^{1,56}\$ Strain sensing by a composite containing Pt nanocrystallites and carbonaceous matrix has been reported, \$^{57}\$ as has gas sensing. \$^{58}\$

FEBID of Pt nanostructures has largely utilized the commercially available CVD precursor (trimethyl)-methylcyclopentadienylplatinum(IV) (MeCpPtMe₃, 1), which is sufficiently volatile for transport as well as being easy to handle due to its air- and water-stability. Despite the excellent performance of Pt complex 1 as a CVD precursor, the deposits generated by FEBID contain impurities from incomplete ligand fragmentation and dissociation. As a result, the deposits are primarily composed of carbon derived from the ligands, with Pt content around 20%. Because many applications, such as electronic devices and catalysts, require nearly pure metal content material, various purification methods have been developed to increase the Pt content in the deposits. These include postdeposition annealing in

Chart 1. Structures of Precursor Complexes Discussed in This Spotlight

1 atm O₂ at 500 °C, resulting in significant enhancement of the Pt content from 15 to 70 at. %.64 Exposure of Pt based structures with a flux of atomic hydrogen for 10 min under 150 °C decreased the carbon content from approximately 81 to 65 at. %. 46 Postdeposition purification has also been achieved by electron-stimulated desorption with the assistance of water vapor. 65 Mechanistic studies under UHV conditions demonstrated that the rate of purification is reliant on the supply of H₂O vapor and concluded that formation of ionized H₂O and •OH radicals is crucial for the purification process.⁶⁶ An attempt to remove the amorphous C matrix from a sub-10 nm wide freestanding Pt nanowire formed by EBID utilized exposure to high energy electrons (200 keV) in a TEM.⁶⁷ These postdeposition purification methods indeed yield material with higher Pt content, 61 but the nanostructure often becomes distorted in shape or highly porous. 62,63,68

Electron-induced reactivity in thin films of precursor 1 has been studied under UHV conditions using various surface analytical techniques, such as temperature-programmed desorption (TPD), X-ray photoelectron spectroscopy (XPS), mass spectrometry (MS), high-resolution electron energy loss

spectroscopy (HREELS), and reflection-absorption infrared spectroscopy (RAIRS). The results have been used to elucidate the electron-induced decomposition of 1 and to rationalize the chemical composition of deposits fabricated by FEBID. Analysis by XPS following electron irradiation of monolayer films of 1 in UHV indicated that the product was a carbonaceous film containing Pt reduced from the original Pt(IV) oxidation state in the precursor to an effective oxidation state close to that of metallic Pt.⁵⁹ During electron irradiation, analysis of the gas phase desorption products by MS revealed precursor fragments with m/z = 2, 15, and 16, which correspond to H₂ and CH₄, respectively. ⁵⁹ The presence of methane is consistent with electron-induced cleavage of a Pt-CH₃ bond in precursor 1, a process that would yield the PtC₈ stoichiometry observed in the final deposit. RAIRS and HREELS studies have shown that electron irradiation also leads to dehydrogenation, ⁶⁹ partially as a result of methane/ methyl radical ejection. Electron stimulated C-H bond cleavage also occurs within the deposits, although these residual C-H bonds remain thermally stable at room temperature. 70 The cross section for electron-induced

decomposition of 1 was determined in parallel TPD, XPS, and MS experiments and was found to depend on the incident energy of the electrons with a maximum between 70 and 100 eV. Two independent temperature-dependent studies have also shown that the composition of the deposits is independent of substrate temperature, indicating that the metal content is determined exclusively by electron-induced reactions. 71,72 The Pt content reported from deposits created using MeCpPtMe₃ without any purification ranges from \sim 16 to 26 at. %. 62 This can be ascribed to the inherent uncertainties in EDXS measurements, which are the usual means of measuring composition, measured in different laboratories and using different instruments under different operating conditions. Moreover, the composition and quantity of background gases (e.g., water vapor, hydrocarbons) in electron microscopes are usually poorly defined and can also influence deposit composition. 26,36 Given the demonstrated ability that water has shown to purify deposits created from MeCpPtMe₃, ^{65,66} it can also be hypothesized that reported differences in the composition of deposits created from this precursor, which typically range from 15 to 25%, are a consequence of different levels of in situ purification caused by residual water vapor in the electron microscopes.²⁶ Indeed, the lack of consistency in deposition conditions and measurement techniques is an issue that has hampered understanding and consistency within the FEBID community.

In an effort to avoid carbon contamination in Pt deposits, the carbon-free precursor tetrakis(trifluorophosphine)platinum(0) (Pt(PF₃)₄, 2) was studied under UHV surface science conditions. 73 The data were consistent with a two stage electron-induced decomposition process, in which a single PF₃ ligand desorbed in the initial electron-stimulated decomposition of the precursor, leading to the formation of an adsorbed Pt(PF₃)₃ intermediate. Subsequent electron-stimulated reactions led to P-F bond cleavage and desorption of the fluorine but phosphorus atoms remained as contaminants in the deposit. However, the Pt(PF₃)₃ intermediates are also susceptible to a degree of PF₃ desorption at room temperature, so electron-stimulated decomposition and thermal desorption of PF₃ are both possible during FEBID. Under these conditions, deposit composition will be sensitive to the deposition conditions (e.g., dwell time, refresh rate, beam fluence) as is found experimentally. The P atoms formed as a result of P-F bond cleavage are highly susceptible to oxidation from water vapor, which provides a rationale for the oxygen frequently observed in deposits created from 2. In terms of postdeposition purification, annealing in an air/N₂ mixture at 200 °C for 30 min has been used to improve the deposit resistivity by factors of 1.6-9.9, depending on the deposition conditions but was associated with a 40% shrinkage of the deposit.⁷⁴ This underscores the advantages of developing precursors that will yield deposits with useful metal purities without the need for postdeposition purification steps.

 $Pt(CO)_2Cl_2$ (3) and $Pt(CO)_2Br_2$ (4) were studied as precursors designed to avoid possible ligand-derived contamination.³² The choice of ligands was based on UHV studies that demonstrated removal of carbonyl and halide ligands in the electron-induced surface reactions of $(\eta^3$ -allyl)Ru- $(CO)_3Br$,⁷⁵ while the anionic polyhapto allyl ligand was a source of carbon contamination in the deposit.²⁵ A UHV surface science study of electron-induced decomposition of a few monolayers of 3 demonstrated a loss of more than 50% of the CO ligands from the precursor surface when irradiated by

lower electron doses ($\lesssim 2 \times 10^{16} \text{ e}^{-/\text{cm}^2}$).³² Upon further electron doses ($\sim 2 \times 10^{16}$ to $\sim 1 \times 10^{17}$ e⁻/cm²), a small amount of CO ligand decomposition to graphitic carbon was observed. However, deposition under steady-state conditions, where the substrate was exposed to a constant flux of precursor, led to complete CO desorption as evidenced by the lack of any observable carbon or oxygen in the deposits. This suggests that when deposition is performed under steadystate conditions with the substrate at room temperature, residual CO groups that do not desorb as a result of the initial electron-stimulated decomposition undergo efficient thermal desorption. A similar phenomenon has been observed for other metal carbonyls used as FEBID precursors.⁷⁶ Electron-induced removal of chlorine ligands via a significantly less efficient electron-stimulated desorption process was also observed. However, higher electron doses (>1 \times 10¹⁹ e⁻/cm²) were required to achieve near complete chlorine removal, which implies that postdeposition electron beam processing would be required to remove chlorine contamination under standard FEBID conditions, where steady state precursor delivery results in continuous coverage of the deposit with new material. Further investigations of purification of FEBID deposits from chloride complex 3⁷⁷ demonstrated that postdeposition processing with electrons removes chlorine from the topmost few nanometers of the deposit but is ineffective in eliminating it from the interior. In contrast, exposure to atomic hydrogen (AH) resulted in efficient purification of the structure with the residual Cl essentially not observable by EDXS.⁷⁷ However, the purification by AH afforded porous material, and it was suggested that such deposits could be interesting as high surface area catalytic structures.

Deposition experiments from the Pt(CO)₂X₂ precursors 3 and 4 in an SEM at HV demonstrated the growth of 3D Ptcontaining nanostructures by FEBID.³⁶ The shape and the growth rate of pillars from 3 and 4 were compared to analogous depositions from commercially available precursor 1. Complex 3 was found to yield the highest growth rate, 0.045 nm³/electron, among those three Pt precursors. Compared to cyclopentadienyl complex 1, the deposits fabricated from 3 had an approximately 2% increase in Pt content. The difference in deposition under different conditions, SEM (HV) with steadystate precursor delivery vs surface science study (UHV) on a few monolayers of precursor, was also addressed. In the UHV experiments, deposits from 3 and 4 contained halogen contamination with minimal carbon content.³² In contrast, the deposits fabricated in HV in the SEM, contained large amounts of carbon but little halide contamination.³⁶ These results emphasize the important role that the deposition conditions (cleanliness of the UHV environment as compared to the significantly higher background pressures characteristic of SEM chambers) can play in determining the chemical composition of FEBID deposits. Indeed, this underscores one of the key challenges in developing a more holistic understanding of FEBID as deposits created in different laboratories and under different conditions and analyzed with different techniques often have markedly different chemical composi-

The commonly used chemotherapy agent cisplatin (Pt- $(NH_3)_2Cl_2$) (5) provides an interesting test of precursor design. ³³ From the point of view of minimizing ligand-derived contamination, cisplatin is carbon free and has a simple set of small ancillary ligands. In addition, the NH₃ ligands have the

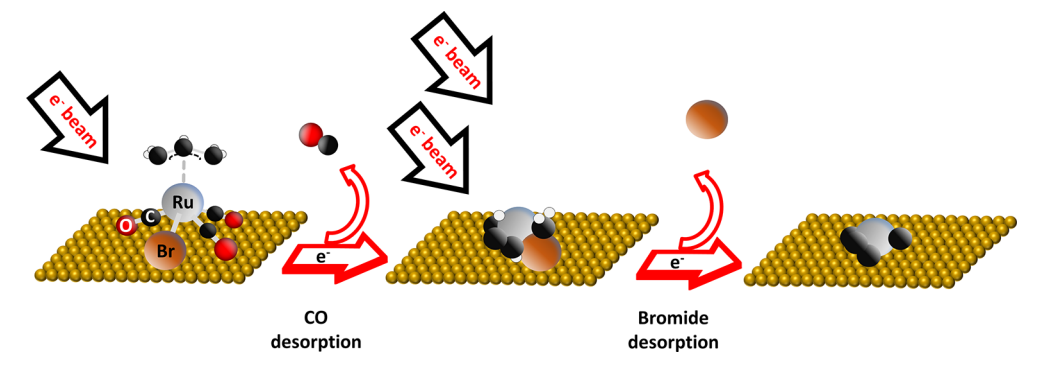


Figure 4. Electron-stimulated desorption of CO, followed by bromide desorption and $(\eta^3 - C_3 H_5)$ decomposition during electron irradiation of 8.

possibility of acting as a reducing agent under electron irradiation by releasing atomic hydrogen. As observed in the treatment of PtCl_x deposits from Pt(CO)₂Cl₂ (3), atomic hydrogen facilitates chlorine removal throughout the deposit structure by forming HCl. 77 Electron irradiation of particles of 5 resulted in the loss of the amine ligands and the formation of nearly pure Pt, consistent with this effect.³³ However, initial FEBID experiments with 5 were hindered by low volatility caused by the presence of polar, H-bonding NH3 ligands in 5 that induce strong intermolecular forces in the crystal. Successful volatilization and transport of 5 for FEBID were achieved using a modified GIS that was heated to 150 °C and featured a short needle and valveless design to avoid clogging during deposition. However, chlorine removal under these conditions was not as efficient as in electron beam irradiation of the cisplatin crystals, with the FEBID deposits from cisplatin vapor containing approximately 50 at. % chlorine. The inefficiency of Cl removal from FEBID of thin films of 5 is attributed to the rapid desorption of NH3 groups which, in the irradiation of crystals, remain trapped long enough to react with Cl ligands and evolve as N_2 and $HCl.^{33}$

There are also reports of the use of ion beams to fabricate Pt nanostructures by FIBID. Pt nanowires fabricated from MeCpPtMe₃ (1) by FIBID with a gallium ion beam⁷⁸ were compared to analogous nanowires grown by FEBID from the same precursor. The FIBID material was found to be 4 orders of magnitude more conductive than the FEBID samples, a result attributed to higher Pt content and Ga doping from the ion beam. FIBID from 1 in a helium ion microscope has been used to fabricate complex 3D mesh structures with a minimum feature size of 16 nm. ⁷⁹ Complex 1 has also been used in cryo-FIBID experiments in which rapid growth of Pt nanostructures was obtained by condensing the precursor onto a cold substrate before patterning with the ion beam instead of using a gas phase delivery system.80 The reduction in fabrication time compared to standard FIBID at room temperature was suggested as a means to enable practical applications.

DEPOSITION OF RU BY FEBID AND FIBID

Fabrication of ruthenium nanostructures has been explored as a means of repairing Ru capping layers in photomasks for EUVL.¹¹ Deposition of Ru-containing nanostructures from bis(ethylcyclopentadienyl)ruthenium(II) (Ru(EtCp)2, 6) was used as a model for potential mask repair technology.¹¹ Because FEBID with 6 produced deposits of the stoichiometry RuC₉, purification by electron-induced reaction with O₂ was explored. Carbon was effectively removed under these

conditions, but the ruthenium was oxidized. More recently, purification of FEBID deposits from 6 using electron-induced reactions with water vapor removed the carbon contamination with minimal oxidation of ruthenium in the initial stages.⁸¹ In contrast, electron-induced reactions of NH3 with FEBID deposits from 6 resulted in nitrogen incorporation to produce amorphous carbon nitride. 82 Although the amount of carbon contamination in FEBID deposits from 6 can be reduced by various purification strategies, efforts to achieve pure Ru deposits through the precursor design are still desirable.

Studies on the allyl complexes $(\eta^3-C_3H_5)Ru(CO)_3Cl$ (7), and $(\eta^3-C_3H_5)Ru(CO)_3Br$ (8) were originally motivated by results from UHV surface science studies of MeCpPtMe₃ (1). 59,61,70 The PtC₈ stoichiometry of the material from electron irradiation of $\mathbf{1}^{59}$ suggested that the η^5 -MeCp ring did not desorb either intact or as fragments and was therefore a source of carbon contamination in the deposit. It was not clear at the time whether anionic π -facial ligands were generally problematic or whether the five metal-carbon bonds in η^5 -MeCp rendered the ligand particularly difficult to remove under FEBID conditions. The η^3 -allyl ligand provided an interesting test of an anionic polyhapto ligand with fewer metal-ligand bonds. Complexes 7 and 8 contain three types of ligands: carbonyl (CO), halogen (Cl, Br), and η^3 -allyl (η^3 -C₃H₅), a ligand set chosen to address not only the lability of the allyl ligand but also the behavior of carbonyl and halide ligands in a heteroleptic complex.⁷⁵ After electron irradiation of a few monolayers of 8 under UHV conditions, the carbons from the polyhapto η^3 -allyl ligand were still present on the surface. In contrast, the carbonyl ligands were ejected into the gas phase, and higher postdeposition electron doses were able to effect partial desorption of bromine from the deposits (Figure 4). 7

Similar results obtained with Cl complex 7 demonstrated that the identity of the halide ligand did not affect the precursor decomposition mechanism. 75 The broader implication from the studies on 7 and 8 on FEBID precursor design is that precursors with a small number of labile and volatile ligands such as carbonyls and halides could result in less contamination from ligand decomposition, which yields higher initial metal content in the deposit and less need for postdeposition purification. In contrast, anionic polyhapto ligands such as allyl and cyclopentadienyl lead to high carbon contents in the deposits and should be avoided.

FEBID studies on complex 8 in an SEM created deposits with 23 at. %. Ru content.83 Postdeposition purification by annealing in forming gas (2% H₂/98% N₂) at 300 °C increased the Ru content to 83 at. %. The ligand-derived impurities were reduced to 13% C and 4% O, with bromine being below detectable limits, as characterized by EDXS and WDS. Although removal of the impurities decreased the volume of the deposit by 79%, its cubic shape was retained. The successful removal of chloride from cisplatin (3) by electroninduced reactions of its ammonia ligands 33,84 inspired purification of deposits from $(\eta^3-C_3H_5)Ru(CO)_3Cl$ (7) by postdeposition reaction with NH3 and electrons to accelerate the removal of surface Cl through the formation of volatile HCl. 85 When deposits made by electron irradiation of thin condensed layers of 7 were subjected to multiple cycles of NH₃ deposition followed by electron exposure (total dose of 3.1 × 10^{17} e⁻/cm² at 31 eV) and periodic annealing to 450 K, the Cl content was reduced by 75% but the procedure was not effective in removing carbon contamination. This result suggests that postdeposition purification with NH3 and electrons can be effective for removing halide ligands from carbon-free deposits, but incorporation of nitrogen has been observed in other studies.82

The observation of electron-induced loss of carbonyl and halide ligands from $(\eta^3-C_3H_5)Ru(CO)_3Br$ (8)⁷⁵ and Pt-(CO)₂Cl₂ (3)³² suggested Ru(CO)₄Br₂ (9) and Ru(CO)₄I₂ (10) as Ru FEBID precursors. UHV surface science studies on the electron-induced reactions of iodide 10 revealed that the reaction proceeded in two stages.⁸⁶ The first stage, at lower electron doses, resulted in the rapid loss of two CO ligands from the substrate surface. The second stage at higher electron doses involved loss of the residual CO ligands in a slower process that afforded a deposit composed of ruthenium and iodine. The identity of the halide ligand was not a factor in electron-induced decomposition, as bromide complex 9 gave similar results. Similar behavior of the different halide complexes was also seen for the $(\eta^3-C_3H_5)Ru(CO)_3X$ complexes 7 and 8.75 FEBID structures made from Ru- $(CO)_4Br_2$ (9) and $Ru(CO)_4I_2$ (10) were found to have the composition of RuX_2 (X = Br, I) (Figure 5), consistent with a general trend for facile removal of multiple carbonyl ligands under electron irradiation, whereas halide removal is relatively slow under the same conditions.

Investigation of iodide 10 as a potential FIBID precursor was carried out in a UHV surface science study using low energy Ar⁺ (860 V).⁸⁷ Figure 6a presents the XPS of 10 upon ion exposure. The O 1s features correspond to the CO ligands. Under ion bombardment, all of the CO ligands desorb as a result of energy transfer from the incident Ar+ ion to the

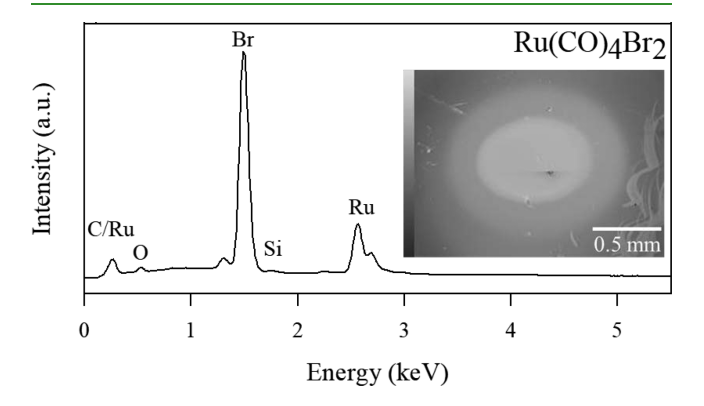


Figure 5. EDXS spectrum of RuBr₂ FEBID deposit created from Ru(CO)₄Br₂. Reproduced with permission from ref 86. Copyright 2020 American Chemical Society.

adsorbed molecules of 10. This process corresponds to the ioninduced decomposition of the precursor as evidenced by the correspondence between the reduction of Ru binding energy and the loss of O 1s intensity seen in Figure 6a. In the XPS analysis of carbon containing Ru species, there is significant overlap between C 1s and Ru 3d features. To quantify the C and Ru content in Figure 6a, we assumed the initial spectrum represented a Ru/C ratio of 0.25, which corresponds to the unreacted precursor 10. Furthermore, the C 1s (289.2 eV) feature of CO overlaps only with the Ru 3d_{3/2} (287.4 eV) feature. The Ru $3d_{5/2}$ (283.2 eV) feature remains unperturbed, and the spin-orbit coupling proportions for photoelectron pairs are known. Therefore, the C 1s and Ru 3d_{3/2} features are resolved using Ru 3d_{5/2} as a basis. After resolving the C 1s and Ru 3d_{3/2} features, the Ru/C ratio is calculated and standardized against the initial C:Ru stoichiometry of complex 10. This quantification method is further supported by mass spectrometry where the decrease in the fractional coverage of CO, as measured by the O 1s peak area, is correlated with the desorption of CO, which is quantified by following the m/z =12 amu. In situ mass spectrometry (Figure 7) demonstrates that ion beam exposure is accompanied by CO desorption and that the rate of CO desorption is proportional to the CO coverage on the surface. This leads to the assertion that the initial Ar⁺-induced process is the decomposition of 10 leading to the dissociation and desorption of all 4 CO ligands (eq 1).

$$Ru(CO)_4I_2(ads) + 860 \text{ eV Ar}^+(g)$$

$$\stackrel{\sigma_1}{\rightarrow} RuI_2(ads) + 4CO(g)\uparrow \qquad (1)$$

As the carbonyl ligands are removed during this precursor decomposition step, the intensities of the Ru 3d and I 3d features remain constant for ion doses up to 0.036 mC/cm². At larger ion doses, the intensity of the Ru 3d and I 3d peaks decreases due to sputtering; however, the I 3d peaks decrease in intensity far more rapidly than the Ru 3d features (Figure 6b). Indeed, the variation in the coverage of Ru, CO and I as a function of Ar+ dose can be described by a sequential series of reactions where initial ion-induced precursor decomposition (eq 1) is followed by preferential Ar+ sputtering of iodine (eq 2) followed by ruthenium (eq 3).

$$RuI_2(ads) + 860 \text{ eV Ar}^+(g) \xrightarrow{\sigma_2} Ru(ads)$$
 (2)

Ru(ads) + 860 eV Ar⁺(g)
$$\xrightarrow{\sigma_3}$$
 clean substrate (3)

The data in Figure 6b were fit to a kinetic model that supports this sequential series of surface reactions, providing a rationale for the clearly visible delay in the onset of Ru loss observed experimentally.⁸⁸ The calculated cross sections indicate that the rate of the initial ion-induced decomposition of iodide complex 10 leading to CO loss is about five times faster than the physical sputtering of I from RuI2, which in turn is itself about five times faster than the rate of Ru sputtering. This sequence of reaction steps indicates that production of pure Ru deposits could be achieved under tailored deposition conditions. These results also highlight the differences that can be found between FEBID (electron beam as energy source) and FIBID (ion beam as energy source) with the same precursor complex 10 (Figure 8). In FIBID, the ion-induced fragmentation of the precursor is accompanied by a greater degree of carbonyl ligand desorption than is observed in

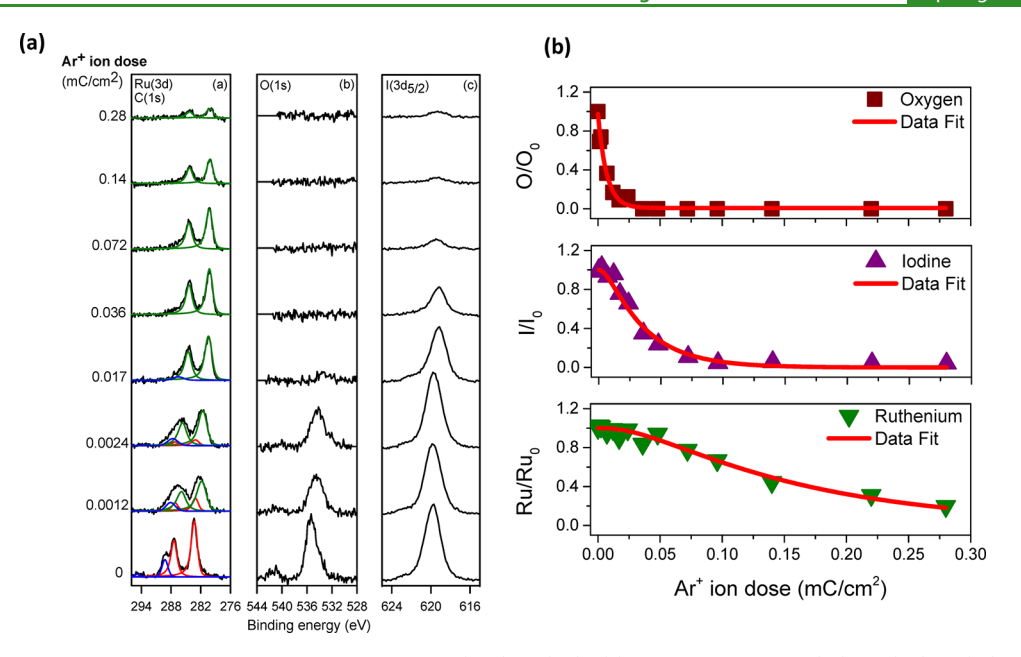


Figure 6. UHV surface study of the ion-stimulated reactions of $Ru(CO)_4I_2$ (10). (a) Evolution of the C(1s)/Ru(3d), O(1s), and $I(3d_{5/2})$ XPS regions for $\sim 1.6-1.7$ nm films of $Ru(CO)_4I_2$ adsorbed onto a Au substrate at -100 °C and exposed to increasing doses of Ar^+ ions. The C(1s)/Ru(3d) region is fit to show contributions clearly from the carbonyl carbon (blue), the initial Ru species (red), and the final Ru species (green). (b) Change in fractional coverage of O, I, and Ru atoms as a function of increasing Ar^+ dose. The solid fits through the data are generated from the kinetic model described in the text. Reproduced with permission from ref 88. Copyright 2020 American Chemical Society.

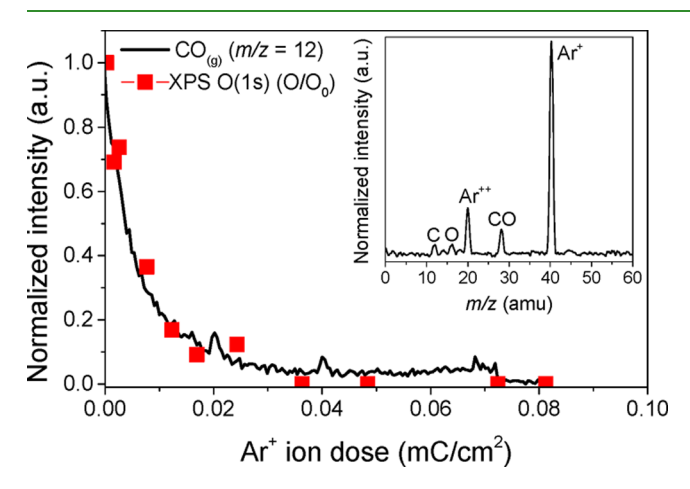


Figure 7. Kinetics of CO desorption from an adsorbed $Ru(CO)_4I_2$ film and its correlation with the fractional coverage of O atoms as observed by XPS. The inset shows the identification of CO as the species desorbing during ion bombardment. Reproduced with permission from ref 88. Copyright 2020 American Chemical Society.

FEBID, followed by ion-induced sputtering of the iodide ligand and then sputtering of the deposited metal atoms.

DEPOSITION OF AU BY FEBID AND FIBID

Interest in FEBID of gold nanostructures has been driven by the changes in the properties of gold when its size reaches the nanoscale. Gold nanoparticles (AuNPs) exhibit unique plasmonic behavior such as high DC conductivity and low ohmic losses, and as a result, AuNPs have found use in a wide range of applications, such as sensing, biological optical imaging, drug delivery, and photothermal therapy (PTT).

Historically, commercially available chemical vapor deposition (CVD) gold precursors, such as $Me_2Au(acac)$ (11), $^{100-102}$ $Me_2Au(tfac)$ (12), 102,103 and $Me_2Au(hfac)$

(13), ¹⁰⁴ were used as gold precursors for FEBID. However, FEBID deposits from those Au(III) precursors are inadequate for use in plasmonic applications due to the high C:Au ratio in the material. ¹⁰⁵ Complete desorption of the bidentate β -diketonate ligands of 11–13 was not observed in UHV surface science studies, ¹⁰⁶ but rather, ligand decomposition under electron irradiation resulted in significant carbon contamination in the deposits. This highlights the general experimental observation that bidentate ligands predominantly undergo decomposition as opposed to desorption during FEBID and should be avoided in precursor design.

Generally, gold nanostructures fabricated by FEBID suffer from unacceptably high levels of carbon contamination, which is a problem for applications such as plasmonics and nanoelectronics. 103,107 Several purification methods can diminish carbon content in deposits. Postdeposition purification by heating FEBID deposits from Me₂Au(tfac) (12) to 500 °C in a reactive atmosphere of oxygen increased the purity from 8 to 60 at. % gold, 64 with TEM analysis indicating the presence of crystalline grains of Au. FEBID from 12 in the presence of coinjected water resulted in a high Au content (91 at. % gold) from in situ purification during the deposition process. 103 The gold nanowires fabricated by this single-step method displayed low resistivities (8.8 $\mu\Omega$ cm) suitable for nanoelectronics. In a related study, high gold content FEBID gold deposits were created from 12 by optimizing the deposition conditions, combined with a postdeposition oxygen-plasma treatment. 107 By increasing the electron dose and optimizing the deposition parameters, Au contents as high as 72 at. % could be obtained before the oxygen-plasma treatment. A postdeposition cleaning process with oxygenplasma further enhanced the Au content from approximately 30 to 70 at. % while largely preserving the structural stability and shape of the original gold deposit; however, the maximum purity of the Au deposit appears to be 73 at. %, as indicated by essentially no change in the Au content in planar Au

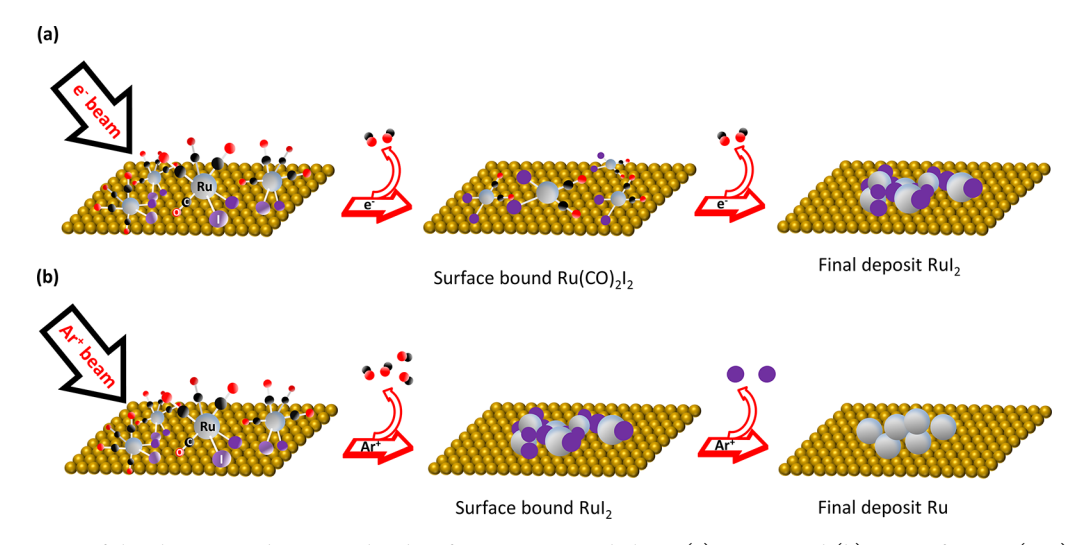


Figure 8. Comparison of the electron- and ion-stimulated surface reactions underlying (a) FEBID and (b) FIBID from $Ru(CO)_4I_2$, respectively. $Ru(CO)_4I_2$ gas phase molecules adsorb to the substrate surface and are exposed to (a) defocused primary electron energy source (500 eV) and (b) defocused Ar^+ ion source (860 V).

nanostructures before (72.5 \pm 0.3 at. %) and after (72.9 \pm 0.3 at. %) oxygen-plasma treatment.

From the perspective of precursor design, an alternative to the four-coordinate Au(III) precursors mentioned above would be two-coordinate Au(I) precursors because lowering the number of ligands is a strategy for minimizing ligand-derived contamination from incomplete ligand desorption during FEBID. Indeed, the Au(I) precursors Cl–Au–PF $_3$ (14) and Cl–Au–CO (15) $^{108-111}$ have been reported to produce high metal content deposits by FEBID. Complex 14 afforded pure metallic gold grains, 112 whereas deposits from 15 were reported to be >95 at. % Au. 111 However, those two Au(I) precursors are sensitive toward temperature, moisture, air, and light. Decomposition of 15 by decarbonylation in the GIS was detected as a pressure spike when the CO was released into the chamber. 111 As a result of their sensitivity to ambient conditions, neither Cl–Au–PF $_3$ (14) nor Cl–Au–CO (15) is acceptable for practical use.

Other Au(I) complexes have been explored to address the precursor stability issue. The two coordinate Au(I) phosphine complexes, Cl–Au–PMe₃ (16) and Me–Au–PMe₃ (17) were studied as potential FEBID precursors. Complex 16 was not sufficiently volatile for FEBID. Although 17 is stable and volatile, only a single methyl ligand was removed under electron irradiation, yielding a deposit with low gold content (19–25 at. %).

To expand the ligand options for gold precursors, we studied CF_3 -Au-CNMe (18) and CF_3 -Au-CN^tBu (19) to introduce CF_3 and alkyl isocyanides as new ligands for FEBID. Isocyanide complexes 18 and 19 are isoelectronic with Cl-Au-CO (15), with both CO and CNR ligands being bound to the metal through carbon lone pairs and the CF_3 group being an anionic electron-withdrawing ligand analogous to a halide. Complexes 18 and 19 were tested with sublimation experiments because of the practical requirement for volatilization and transport through a GIS without decomposition. The sublimation experiment was conducted with a modified Schlenk line equipped with a pressure controller to hold the vacuum constant at 125 \pm 1 mTorr. Under these conditions, 18 and 19 were sufficiently volatile and thermally stable to sublime at 51 and 39 °C, respectively. The electron-

induced reactions of **18** and **19** were studied using energy-dispersive X-ray spectroscopy (EDXS) and Auger electron spectroscopy (AES). EDX spectra provided elemental composition analyses of the deposits. The C:Au ratios of precursors **18**, **19**, and **11** are 3:1, 6:1, and 7:1 from the stoichiometry of these precursors, respectively. The C:Au of the deposits from **18** and **19** were determined to be 2.8:1 and 5.7:1, respectively, from the EDX spectra. Fluorine loss was the dominant desorption pathway, along with minimal loss of the carbons from the ligands. Deposits formed from **18** had Au contents of 22 at. %, comparable to those from FEBID with the commercial precursor **11**. 113,114

Although the halide derivatives XAuCNR did not prove to be practical precursors for FEBID, 115 they were included in a study of the effects of halide choice on volatility and stability of potential Au(I) precursor candidates. For the X–Au–L complexes [X = Cl, Br, I; L = CNtBu, CNMe, PMe3, P(NMe2)3, P(OCH2CF3)3], the iodide complexes were the most volatile of the three in each series. The volatility trends could be explained using the variation of the Au–Au bond distances caused by aurophilic interactions and the aggregation of molecules in the solid state. It was concluded that for potential Au(I) FEBID precursors of the type X-Au-L, the stability and volatility could be controlled by ligand choice of X and L (Figure 9). Thermal stability was most affected by the σ -donor properties of the two-electron donor ligand L, whereas the size of the X group was critical for volatility.

Efforts to extend the use of strong σ -donor ligands in Au(I) FEBID precursors led to the use of N-heterocyclic carbene (NHC) ligands in a series of X-Au(NHC) complexes. ¹¹⁶ Variations in the NHC ring (imidazole or triazole) and the N-alkyl substituents (Me, Et, $^{\rm i}$ Pr) were examined and it was

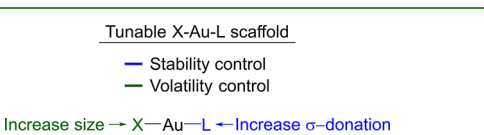


Figure 9. Tuning XAuL complexes for increased stability and volatility. Reproduced with permission from ref 113. Copyright 2019 American Chemical Society.

concluded that the triazole derivatives were most promising. The volatility of these complexes was too low for use in a standard GIS, so the FEBID experiments required construction of a custom precursor delivery system, in which the complex was volatilized from crystals placed directly on a heated substrate. FEBID under those conditions from the Cl– Au(NHC) complex where NHC = N,N'-diethyltriazole (20) afforded deposits that were 15 at. % gold. 116

Deposition of gold by FIBID has also been reported. Films that were 55% gold and 45% carbon were deposited on a quartz-crystal microbalance upon ion bombardment of Me₂Au(hfac) (13), with Ar⁺, Kr⁺, or Xe⁺ at energies of 2-10 keV. The effect of the ion species (He⁺, Ne⁺, Ar⁺, Kr⁺, and Xe⁺) and energies on FIBID of 13 was investigated and the results were consistent with a binary collision model for precursor decomposition. 117,118 Higher gold contents up to 80 at. % were obtained with higher energy (50-100 keV) Kr+ or Xe+ ions. 118 A high-purity gold deposit was created by using a focused Ga+ ion beam (15 keV, 0.5 µm diameter) in FIBID with gold complex 13. 119 Although the deposit was 75 at % gold and less than <5 at. % carbon and oxygen, the material was contaminated with 15-20 at. % Ga. This result demonstrates that the choice of ion beam has implications for the composition of the deposited material, and Ga+ is less desirable for applications where impurities are problematic.

In general, because of the mass differences of the ions, using different ions in FIBID will affect various aspects of deposition, such as imaging resolution, secondary electron yield, sputter yield, and ion implantation into the deposit. Because of their low mass, He+ ions have a narrow interaction volume that is desirable for microscopy, but undesirable for FIBID processes. Ar+ and Ne+ can generate adequate amounts of secondary electrons in low beam energies (30 keV). Compared to He⁺ the beam penetration depth of Ar⁺ and Ne⁺ is shallower, which reduces the ion-substrate interactions. To the best of our knowledge, Kr⁺ and Xe⁺ are rarely used for FIBID given the greater availability of Ar and similar ion penetration depths of Ar⁺ (10 nm) and Ga⁺ (8 nm). Heavier ions have a greater sputtering yield than lighter ions, which could be detrimental for deposit formation but can also have the advantage of removing light atom impurities. 120 This effect has been noted in a comparison of different ion sources in FIBID of Sn films from tetramethyltin (TMT), which has a Sn:C ratio of 1:4 in the precursor. 121 Although deposits made using 50 keV H2+ ions had a 1:3.5 Sn:C ratio that was nearly equal to the stoichiometry of the precursor, films made using 30 keV Ar+ ions had a Sn:C ratio of only 1:1.6.

■ DEPOSITION OF FE-CONTAINING ALLOYS BY FEBID AND FIBID

Iron alloy nanostructures have recently been of great interest because of their magnetic properties and potential uses in magnetics, spintronics, and thermoelectrics. Developing methods to fabricate alloy deposits by FEBID and/or FIBID is the key for further extension of the application range to multimetallic lithography materials. When single-metal precursors are available, it is possible to generate alloys by injecting different gas-phase precursors in parallel but the different volatilities, transport properties, adsorption, and reactivities of the two precursors can make process optimization and control difficult. Simultaneous introduction of two species can be done by either using a single GIS to introduce a mixture of the two precursors

GISs that inject the precursors separately. The latter method has been used when simultaneous stoichiometric introduction of the precursors resulted in problems with controlling the stoichiometry of the material, because of preferential adsorption of one precursor. As an example, FeSi and Fe₃Si were made by alternating the introduction of Fe(CO)₅ (21) and Si₅H₁₂ (22) to create a multilayer structure, which was then irradiated with an electron beam and annealed to enable intermixing. 122

As a result of the challenges inherent in using mixtures of precursors, there has been recent interest in heterometallic single-source complexes as FEBID and FIBID precursors to facilitate fabrication of alloy nanostructures with controlled deposit stoichiometry. The use of heterobimetallic complexes and larger clusters as precursors can also be challenging because the weakness of their metal-metal bonds and the low volatilities that can result from high molecular weights limit the number of compounds that will volatilize before decomposition. At this point, exploratory studies of heterometallic compounds also require synthetic effort because they are not generally commercially available, but there are promising results among the reported studies. The cluster complex HFeCo₃(CO)₁₂ (23) was the first successful bimetallic singlesource precursor for FEBID. 123 Deposits from 23 had an unusually high metal content for metal carbonyl precursors (>80 at. %) and maintained a stoichiometric Fe:Co metal ratio (1:3) upon electron irradiation. Successful FEBID of ferromagnetic alloy nanostructures from 23 motivated study of the FeRu cluster H₂FeRu₃(CO)₁₃ (24).⁴¹ Surprisingly, FEBID deposits from 24 contained a much lower metal content of around 26 at. %. A comparison of clusters 23 and 24 in UHV surface science studies provided insight into their differences.⁴¹ Electron irradiation of the FeCo cluster 23 resulted in initial desorption of 75% of the CO ligands. 126 UHV studies also revealed that when deposition occurred at room temperature, the remaining CO ligands could undergo desorption to afford deposits that were almost free of carbon and oxygen impurities (Figure 10). In contrast, the UHV study of FeRu cluster 24 demonstrated the desorption of 8-9 CO ligands during the electron-induced decomposition of the precursor, but the partially decarbonylated intermediates that formed were inert to either further electron irradiation or annealing to room temperature and would therefore likely be incorporated in the deposits. 41 Thus, the crucial difference between 23 and 24 was postulated to be the thermal stability of the partially decarbonylated intermediates produced upon initial electron irradiation.

The heterobimetallic complex $(\eta^5 - C_5H_5)Fe(CO)_2Mn(CO)_5$ (25) was studied under UHV surface science conditions as a possible FEBID precursor for FeMn alloy nanostructures. 127 A goal of these studies was to investigate electron-induced carbonyl loss in a complex where the metal oxidation states and coordination spheres were different because of the presence of the anionic polyhapto cyclopentadienyl ligand. Upon irradiation in UHV with low doses of electrons, the precursor was decarbonylated until the O:C ratio determined by XPS was consistent with desorption of roughly 5 CO ligands of the 7 per molecule (Figure 11). More extensive electron doses resulted in decomposition of the remaining CO ligands and the cyclopentadienyl (η^5 -C₅H₅) ligand to afford graphitic carbon and reactive oxygen species (ROS) that were responsible for the selective oxidation of Mn atoms. The lack of Fe oxidation was attributed to the presence of the

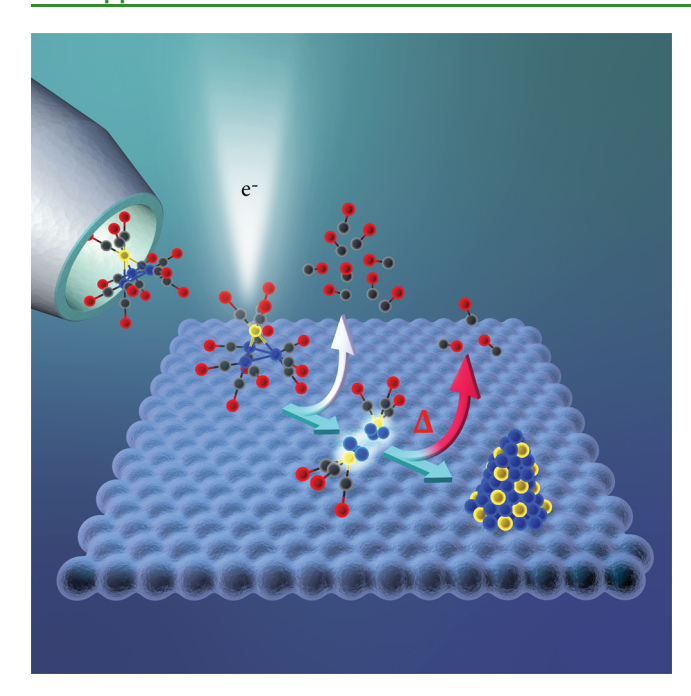


Figure 10. Proposed mechanisms for the decomposition of HFeCo₃(CO)₁₂ (23) during FEBID. Initial electron-induced decomposition of the precursor results in desorption of 75% of the CO ligands (white arrows), followed by thermal desorption of the remaining carbonyls (red arrows) from the partially decarbonylated intermediates to produce FeCo₃ deposits. Reproduced with permission from ref 126. Copyright 2018 American Chemical Society.

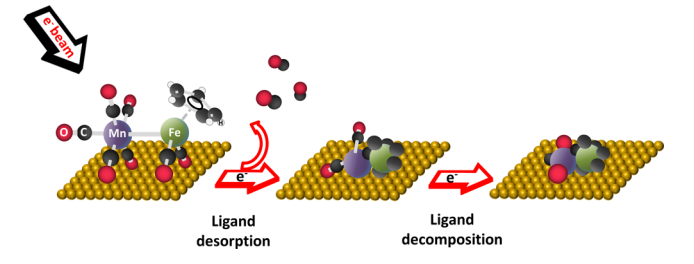


Figure 11. Electron-stimulated CO desorption from $(\eta^5\text{-}\text{C}_5\text{H}_5)\text{Fe}(\text{CO})_2\text{Mn}(\text{CO})_5$ (25) followed by electron-stimulated decomposition of the $\eta^5\text{-}\text{C}_5\text{H}_5$ (Cp) ring and the residual CO groups that do not desorb during the initial deposition process.

cyclopentadienyl ring but subsequent studies on the analogous FeRe complex $(\eta^5\text{-}\mathrm{C}_5\mathrm{H}_5)\mathrm{Fe(CO)}_2\mathrm{Re(CO)}_5$ $(26)^{87}$ (vide infra) bring that conclusion into question. Deposits fabricated from 25 under steady-state conditions in an Auger spectrometer were heavily contaminated with C (51 at. %) and O (13 at. %) but the Fe:Mn ratio was 1:1 (18 at. % each), consistent with the initial stoichiometry of the metals in 25, providing evidence that the stoichiometry of alloys can be controlled by using heterobimetallic precursors to fabricate nanostructures using FEBID. 127

The related heterobimetallic precursor $(\eta^5-C_5H_5)$ Fe- $(CO)_2$ Re $(CO)_5$ (26) has the same electronic structure as 25 but contains the third row transition metal Re as a congener of Mn in the M(CO)₅ fragment. In the UHV surface science study of the electron-induced reactions of 26,⁸⁷ half of the CO ligands were desorbed under lower electron doses. Further electron irradiation led to decomposition of the remaining CO ligands and the Cp ring into species that were retained in the material.⁸⁷ There are some similarities in the electron-induced

reactions of 25 and 26. For both, two stages of precursor decomposition were evident, as shown for 25 in Figure 12. In

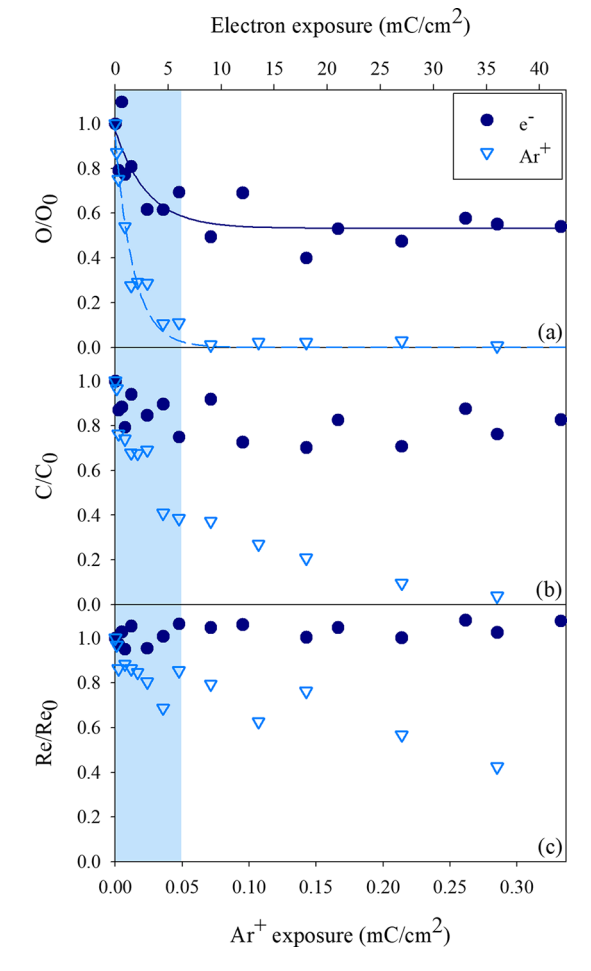


Figure 12. Changes in the fractional coverage of oxygen, carbon, and rhenium atoms upon electron (dark circles, top x axis) and argon ion (light open triangles, bottom x axis) exposure of thin films of $(\eta^5 - C_5H_5)Fe(CO)_2Re(CO)_5$ (26). The changes in composition, which occur during the initial region of the electron (\sim 6.0 mC/cm²) or argon ion (\sim 0.048 mC/cm²) exposure are denoted by the blue shaded region. Reproduced with permission from ref 87. Copyright 2020 American Chemical Society.

the first stage (lower electron doses) multiple carbonyls desorb and in the second stage (higher electron doses), CO and Cp fragmentation afford C and O content in the resulting deposit. These similarities are mirrored in the behavior of other precursors that contain multiple CO ligands and anionic carbon ligands. The difference in the behavior of 25 and 26 under electron irradiation lies in the site of reactivity for the ROS generated from decomposition of carbonyls. The oxidation of 25 occurs at Mn and the binding energies of Fe are largely unchanged, while in 26, the Fe centers are preferentially oxidized.

An analogous study of the ion beam-induced reactions of FeRe complex **26** under UHV conditions⁸⁷ revealed significant differences from the electron-induced reactions that have important implications for FEBID/FIBID precursors. Upon bombardment with an Ar⁺ ion beam (860 V), all of the CO ligands desorbed as a result of energy transfer from the incident ions. Subsequent ion-induced sputtering of the deposit preferentially removed the remaining precursor

carbons, with metal atoms undergoing slower removal. Figure 12 contrasts the removal of precursor atoms from 26 under electron irradiation (dark circles) with ion-induced removal (light triangles). For ion doses >0.2 mC/cm², the deposits are almost purely metallic. These results suggest that for precursors that undergo incomplete ligand desorption during FEBID, a switch to FIBID could lead to high metal content deposits from the same precursor due to the balance between ion-induced deposition and preferential sputtering of light atoms during FIBID (Figure 13).

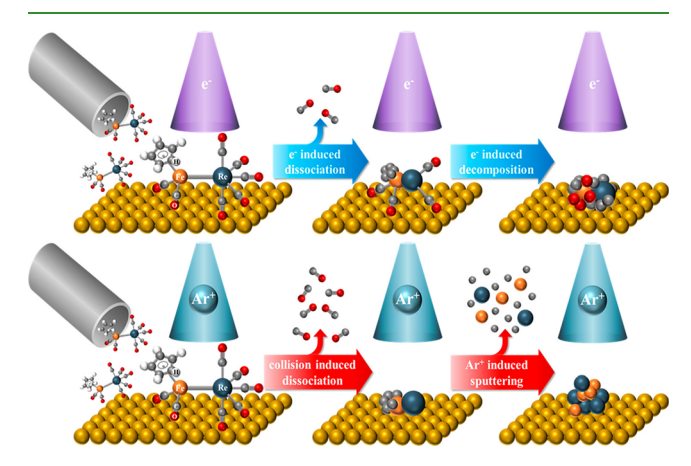


Figure 13. Schematic representation of the sequence of molecular-level events that accompany the 500 eV electron (top) and 860 eV Ar⁺ ion (bottom) exposure of adsorbed (η⁵-C₅H₅)Fe(CO)₂Re(CO)₅ (**26**) on a gold substrate. Reproduced with permission from ref 87. Copyright 2020 American Chemical Society.

CONCLUSION

Although FEBID and FIBID have been demonstrated to fabricate complex 3D metal nanostructures for a variety of applications, there are still limitations due to the incorporation of ligand-derived impurities in the deposits. The metal percentage in FEBID/FIBID fabricated objects is dependent on the composition of the precursor and its reaction pathways during electron- and ion-induced chemistry. UHV surface science studies of charged particle-induced reactions provide an important means to identify mechanistic steps for ligand dissociation and decomposition. In this way, privileged ligands that leave minimal contamination in the deposits can be identified.

This spotlight presents case studies of Pt, Ru, Au, and heterometallic organometallic complexes as FEBID/FIBID precursors that lead to the following general conclusions about precursor design:

- 1. Organometallic precursors should contain a minimum number of small ligands for both FEBID and FIBID.
- CO ligands desorb well and are good candidates for both FEBID and FIBID. Desorption of multiple (2-3) CO ligands is common during FEBID and desorption of all CO ligands is possible with FIBID.
- 3. The presence of NH₃ ligands during FEBID can assist with halide removal through the formation of HX species upon electron irradiation. However, the hydrogen bonding associated with the NH₃ ligand can result in low volatility.

- Halide ligands are removed slowly (and often partially) during FEBID but can be removed completely during FIBID due to sputtering.
- 5. Anionic ligands that are polyhapto or bidentate are difficult to completely remove during FEBID and FIBID and decompose into fragments that are incorporated as impurities. Although they can ultimately be removed by the preferential sputtering of light atoms in metal deposits during FIBID, it comes at the cost of removing a substantial fraction of the deposited metal atoms as well.
- 6. Heterometallic single-source precursors are good candidates for deposition of alloys by FEBID and FIBID. Because unsupported metal—metal bonds are weak and the molecular weights tend to be high, heterobimetallics and mixed-metal clusters that volatilize before decomposition may be difficult to identify. Ligands used to optimize structural properties may be more easily removed by FIBID.

As mechanistic data from UHV experiments continue to accumulate, additional privileged ligands and structure—activity relationships for charged particle-induced reactions will be identified, providing a base for mechanism-based precursor design for FEBID and FIBID.

AUTHOR INFORMATION

Corresponding Author

Lisa McElwee-White — Department of Chemistry, University of Florida, Gainesville, Florida 32611-7200, United States; orcid.org/0000-0001-5791-5146; Email: lmwhite@chem.ufl.edu

Authors

Jo-Chi Yu – Department of Chemistry, University of Florida, Gainesville, Florida 32611-7200, United States

Mohammed K. Abdel-Rahman – Department of Chemistry, Johns Hopkins University, Baltimore, Maryland 21218-2685, United States

D. Howard Fairbrother – Department of Chemistry, Johns Hopkins University, Baltimore, Maryland 21218-2685, United States; orcid.org/0000-0003-4405-9728

Complete contact information is available at: https://pubs.acs.org/10.1021/acsami.1c12327

Notes

The authors declare no competing financial interest.

ACKNOWLEDGMENTS

L.M.W. and D.H.F. thank the National Science Foundation for support of this work through the linked collaborative grants CHE-1607621, CHE-1904559 and CHE-1607547, CHE-1904802. The names of the talented group of students and postdocs who have participated in this project over many years can be found in the references. We also thank our collaborators supported within the framework of ELENA, a European Union's Horizon 2020 research and innovation program under the Marie Skłodowska-Curie grant agreement 722149.

REFERENCES

(1) Huth, M.; Porrati, F.; Dobrovolskiy, O. V. Focused Electron Beam Induced Deposition Meets Materials Science. *Microelectron. Eng.* **2018**, 185–186, 9–28.

- (2) Huth, M.; Porrati, F.; Schwalb, C.; Winhold, M.; Sachser, R.; Dukic, M.; Adams, J.; Fantner, G. Focused Electron Beam Induced Deposition: A Perspective. *Beilstein J. Nanotechnol.* **2012**, *3*, 597–619.
- (3) Utke, I.; Hoffmann, P.; Melngailis, J. Gas-assisted Focused Electron Beam and Ion Beam Processing and Fabrication. *J. Vac. Sci. Technol.*, B **2008**, 26 (4), 1197–1276.
- (4) Plank, H.; Winkler, R.; Schwalb, C. H.; Hütner, J.; Fowlkes, J. D.; Rack, P. D.; Utke, I.; Huth, M. Focused Electron Beam-Based 3D Nanoprinting for Scanning Probe Microscopy: A Review. *Micromachines* 2020, 11 (1), 48.
- (5) Utke, I.; Moshkalev, S.; Russell, P. Nanofabrication Using Focused Ion and Electron Beams: Principles and Applications; Oxford University Press: 2012.
- (6) Edinger, K.; Becht, H.; Bihr, J.; Boegli, V.; Budach, M.; Hofmann, T.; Koops, H. W. P.; Kuschnerus, P.; Oster, J.; Spies, P.; Weyrauch, B. Electron-beam-Based Photomask Repair. J. Vac. Sci. Technol., B: Microelectron. Process. Phenom. 2004, 22 (6), 2902–2906.
- (7) Liang, T.; Frendberg, E.; Lieberman, B.; Stivers, A. Advanced Photolithographic Mask Repair Using Electron Beams. *J. Vac. Sci. Technol., B: Microelectron. Process. Phenom.* **2005**, 23 (6), 3101–3105.
- (8) Heerkens, C. T. H.; Kamerbeek, M.; van Dorp, W.; Hagen, C.; Hoekstra, J. Electron Beam Induced Deposited Etch Masks. *Microelectron. Eng.* **2009**, *86* (4), 961–964.
- (9) Bret, T.; Hofmann, T.; Edinger, K. Industrial Perspective on Focused Electron Beam-Induced Processes. *Appl. Phys. A: Mater. Sci. Process.* **2014**, *117* (4), 1607–1614.
- (10) Yan, P.-y.; Spiller, E.; Mirkarimi, P. Characterization of Ruthenium Thin Films as Capping Layer for Extreme Ultraviolet Lithography Mask Blanks. *J. Vac. Sci. Technol., B* **2007**, 25 (6), 1859—1866
- (11) Noh, J. H.; Stanford, M. G.; Lewis, B. B.; Fowlkes, J. D.; Plank, H.; Rack, P. D. Nanoscale Electron Beam-Induced Deposition and Purification of Ruthenium for Extreme Ultraviolet Lithography Mask Repair. *Appl. Phys. A: Mater. Sci. Process.* **2014**, *117* (4), 1705–1713.
- (12) Hubner, B.; Koops, H. W. P.; Pagnia, H.; Sotnik, N.; Urban, J.; Weber, M. Tips for Scanning Tunneling Microscopy Produced by Electron-beam-induced Deposition. *Ultramicroscopy* **1992**, 42–44, 1519–1525.
- (13) Chen, I.-C.; Chen, L.-H.; Orme, C.; Quist, A.; Lal, R.; Jin, S. Fabrication of High-Aspect-Ratio Carbon Nanocone Probes by Electron Beam Induced Deposition Patterning. *Nanotechnology* **2006**, *17* (17), 4322–4326.
- (14) Graells, S.; Alcubilla, R.; Badenes, G.; Quidant, R. Growth of Plasmonic Gold Nanostructures by Electron Beam Induced Deposition. *Appl. Phys. Lett.* **2007**, *91* (12), 121112.
- (15) Weber-Bargioni, A.; Schwartzberg, A.; Schmidt, M.; Harteneck, B.; Ogletree, D.; Schuck, P.; Cabrini, S. Functional Plasmonic Antenna Scanning Probes Fabricated by Induced-Deposition Mask Lithography. *Nanotechnology* **2010**, *21* (6), 065306.
- (16) Koops, H. W. P.; Hoinkis, O. E.; Honsberg, M. E. W.; Schmidt, R.; Blum, R.; Bottger, G.; Kuligk, A.; Liguda, C.; Eich, M. Two-dimensional Photonic Crystals Produced by Additive Nanolithography with Electron Beam-Induced Deposition Act as Filters in the Infrared. *Microelectron. Eng.* **2001**, *57*–8, 995–1001.
- (17) Gonzalez, C. M.; Timilsina, R.; Li, G.; Duscher, G.; Rack, P. D.; Slingenbergh, W.; van Dorp, W. F.; De Hosson, J. T. M.; Klein, K. L.; Wu, H. M.; Stern, L. A. Focused Helium and Neon Ion Beam Induced Etching for Advanced Extreme Ultraviolet Lithography Mask Repair. J. Vac. Sci. Technol., B: Nanotechnol. Microelectron.: Mater., Process., Meas., Phenom. 2014, 32 (2), 021602.
- (18) Sato, T.; Aizawa, Y.; Matsumoto, H.; Kiyohara, M.; Kamiya, C.; von Cube, F. Low Damage Lamella Preparation of Metallic Materials by FIB Processing with Low Acceleration Voltage and a Low Incident Angle Ar Ion Milling Finish. *J. Microsc.* **2020**, 279 (3), 234–241.
- (19) Córdoba, R.; Orús, P.; Strohauer, S.; Torres, T. E.; De Teresa, J. M. Ultra-fast Direct Growth of Metallic Micro-and Nano-Structures by Focused Ion Beam Irradiation. *Sci. Rep.* **2019**, *9* (1), 1–10.

- (20) Kim, C.-S.; Ahn, S.-H.; Jang, D.-Y. Review: Developments in Micro/Nanoscale Fabrication by Focused Ion Beams. *Vacuum* **2012**, *86* (8), 1014–1035.
- (21) Drezner, Y.; Fishman, D.; Greenzweig, Y.; Raveh, A. Characterization of damage induced by FIB etch and tungsten deposition in high aspect ratio vias. J. Vac. Sci. Technol., B: Nanotechnol. Microelectron.: Mater., Process., Meas., Phenom. 2011, 29 (1), 011026.
- (22) Li, P.; Chen, S.; Dai, H.; Yang, Z.; Chen, Z.; Wang, Y.; Chen, Y.; Peng, W.; Shan, W.; Duan, H. Recent Advances in Focused Ion Beam Nanofabrication for Nanostructures and Devices: Fundamentals and Applications. *Nanoscale* **2021**, *13* (3), 1529–1565.
- (23) Belianinov, A.; Burch, M. J.; Kim, S.; Tan, S.; Hlawacek, G.; Ovchinnikova, O. S. Noble Gas Ion Beams In Materials Science for Future Applications and Devices. MRS Bull. 2017, 42 (9), 660–666.
- (24) Carden, W. G.; Lu, H.; Spencer, J. A.; Fairbrother, D. H.; McElwee-White, L. Mechanism-Based Design of Precursors for Focused Electron Beam-Induced Deposition. *MRS Commun.* **2018**, 8 (2), 343–357.
- (25) Spencer, J.; Rosenberg, S.; Barclay, M.; Wu, Y.-C.; McElwee-White, L.; Fairbrother, D. H. Understanding the Electron Stimulated Surface Reactions of Organometallic Complexes to Enable Design of Precursors for Electron Beam Induced Deposition. *Appl. Phys. A: Mater. Sci. Process.* **2014**, *117*, 1631–1644.
- (26) Barth, S.; Huth, M.; Jungwirth, F. Precursors for Direct-Write Nanofabrication With Electrons. *J. Mater. Chem. C* **2020**, 8 (45), 15884–15919.
- (27) McElwee-White, L. Design of Precursors for the CVD of Inorganic Thin Films. *Dalton Transactions* **2006**, No. 45, 5327–5333.
- (28) Devi, A. 'Old Chemistries' for New Applications: Perspectives for Development of Precursors for MOCVD and ALD Applications. *Coord. Chem. Rev.* **2013**, 257 (23–24), 3332–3384.
- (29) Koponen, S. E.; Gordon, P. G.; Barry, S. T. Principles of Precursor Design for Vapour Deposition Methods. *Polyhedron* **2016**, 108, 59–66.
- (30) Prabhudesai, V. S.; Kelkar, A. H.; Nandi, D.; Krishnakumar, E. Functional Group Dependent Site Specific Fragmentation of Molecules by Low Energy Electrons. *Phys. Rev. Lett.* **2005**, 95 (14), 143202.
- (31) Cotton, F. A.; Wilkinson, G.; Murillo, C.; Bochmann, M. Advanced Inorganic Chemistry, 6th ed.; Wiley: New York, 1999.
- (32) Spencer, J. A.; Wu, Y. C.; McElwee-White, L.; Fairbrother, D. H. Electron Induced Surface Reactions of cis-Pt(CO)₂Cl₂: A Route to Focused Electron Beam Induced Deposition of Pure Pt Nanostructures. *J. Am. Chem. Soc.* **2016**, *138* (29), 9172–82.
- (33) Warneke, J.; Rohdenburg, M.; Zhang, Y.; Orszagh, J.; Vaz, A.; Utke, I.; De Hosson, J. T. M.; van Dorp, W. F.; Swiderek, P. Role of NH₃ in the Electron-Induced Reactions of Adsorbed and Solid Cisplatin. *J. Phys. Chem. C* **2016**, *120* (7), 4112–4120.
- (34) Mîinea, L. A.; Suh, S.; Hoffman, D. M. Indium Fluoroalkoxide Compounds. *Inorg. Chem.* **1999**, 38 (20), 4447–4454.
- (35) Carden, W.; Pedziwiatr, J.; Abboud, K. A.; McElwee-White, L. Halide Effects on the Sublimation Temperature of X-Au-L Complexes: Implications for Their Use as Precursors in Vapor Phase Deposition Methods. ACS Appl. Mater. Interfaces 2017, 9, 40998–41005.
- (36) Mahgoub, A.; Lu, H.; Thorman, R. M.; Preradovic, K.; Jurca, T.; McElwee-White, L.; Fairbrother, H.; Hagen, C. W. Electron Beam-Induced Deposition of Platinum from Pt(CO)₂Cl₂ and Pt(CO)₂Br₂. Beilstein J. Nanotechnol. **2020**, 11, 1789–1800.
- (37) Silvis-Cividjian, N.; Hagen, C. W.; Kruit, P. Spatial Resolution Limits in Electron-Beam-Induced Deposition. *J. Appl. Phys.* **2005**, *98* (8), 084905.
- (38) Botman, A.; de Winter, D. A. M.; Mulders, J. J. L. Electron-Beam-Induced Deposition of Platinum At Low Landing Energies. *J. Vac. Sci. Technol., B* **2008**, 26 (6), 2460–2463.
- (39) Thorman, R. M.; Kumar T P, R.; Fairbrother, D. H.; Ingolfsson, O. The Role of Low-Energy Electrons in Focused Electron Beam

- Induced Deposition: Four Case Studies of Representative Precursors. *Beilstein J. Nanotechnol.* **2015**, *6*, 1904–1926.
- (40) Thorman, R. M.; Brannaka, J. A.; McElwee-White, L.; Ingólfsson, O. Low Energy Electron-Induced Decomposition of $(\eta^3 C_3H_5)$ Ru(CO)₃Br, a Potential Focused Electron Beam Induced Deposition Precursor With a Heteroleptic Ligand Set. *Phys. Chem. Chem. Phys.* **2017**, 19 (20), 13264–13271.
- (41) Kumar T P, R.; Weirich, P.; Hrachowina, L.; Hanefeld, M.; Bjornsson, R.; Hrodmarsson, H. R.; Barth, S.; Fairbrother, D. H.; Huth, M.; Ingólfsson, O. Electron Interactions with the Heteronuclear Carbonyl Precursor H₂FeRu₃(CO)₁₃ and Comparison with HFe-Co₃(CO)₁₂: from Fundamental Gas Phase and Surface Science Studies to Focused Electron Beam Induced Deposition. *Beilstein J. Nanotechnol.* **2018**, *9*, 555–579.
- (42) Kumar T P, R.; Bjornsson, R.; Barth, S.; Ingolfsson, O. Formation and Decay of Negative Ion States up to 11 eV Above the Ionization Energy of the Nanofabrication Precursor HFeCo₃(CO)₁₂. *Chem. Sci.* **2017**, *8*, 5949.
- (43) Engmann, S.; Stano, M.; Matejcik, S.; Ingolfsson, O. The Role of Dissociative Electron Attachment in Focused Electron Beam Induced Processing: A Case Study on Cobalt Tricarbonyl Nitrosyl. *Angew. Chem., Int. Ed.* **2011**, *50* (40), 9475–9477.
- (44) Kopyra, J.; Koenig-Lehmann, C.; Bald, I.; Illenberger, E. A Single Slow Electron Triggers the Loss of Both Chlorine Atoms from the Anticancer Drug Cisplatin: Implications for Chemoradiation Therapy. *Angew. Chem., Int. Ed.* **2009**, 48 (42), 7904–7907.
- (45) Indrajith, S.; Rousseau, P.; Huber, B. A.; Nicolafrancesco, C.; Domaracka, A.; Grygoryeva, K.; Nag, P.; Sedmidubská, B.; Fedor, J.; Kočišek, J. Decomposition of Iron Pentacarbonyl Induced by Singly and Multiply Charged Ions and Implications for Focused Ion Beam-Induced Deposition. *J. Phys. Chem. C* 2019, 123 (16), 10639–10645.
- (46) Botman, A.; Hesselberth, M.; Mulders, J. J. L. Improving The Conductivity of Platinum-Containing Nano-Structures Created by Electron-Beam-Induced Deposition. *Microelectron. Eng.* **2008**, *85*, 1139–1142.
- (47) Wang, Z.; Li, Q.; Besenbacher, F.; Dong, M. Facile Synthesis of Single Crystal PtSe2 Nanosheets for Nanoscale Electronics. *Adv. Mater.* **2016**, 28 (46), 10224–10229.
- (48) Le-The, H.; Küchler, C.; van den Berg, A.; Bodenschatz, E.; Lohse, D.; Krug, D. Fabrication of Freestanding Pt Nanowires for Use as Thermal Anemometry Probes in Turbulence Measurements. *Microsystems & Nanoengineering* **2021**, 7 (1), 28.
- (49) Yang, M.; Qu, F.; Lu, Y.; He, Y.; Shen, G.; Yu, R. Platinum Nanowire Nanoelectrode Array for the Fabrication of Biosensors. *Biomaterials* **2006**, *27* (35), 5944–5950.
- (50) Liang, H. W.; Cao, X.; Zhou, F.; Cui, C. H.; Zhang, W. J.; Yu, S. H. A Free-Standing Pt-Nanowire Membrane as a Highly Stable Electrocatalyst for the Oxygen Reduction Reaction. *Adv. Mater.* **2011**, 23 (12), 1467–1471.
- (51) Chauhan, B. P. S.; Rathore, J. S. Regioselective Synthesis of Multifunctional Hybrid Polysiloxanes Achieved by Pt-Nanocluster Catalysis. *J. Am. Chem. Soc.* **2005**, *127* (16), 5790–5791.
- (52) Liu, L.; Corma, A. Metal Catalysts for Heterogeneous Catalysis: From Single Atoms to Nanoclusters and Nanoparticles. *Chem. Rev.* **2018**, *118* (10), 4981–5079.
- (53) Narayanan, R.; El-Sayed, M. A. Shape-Dependent Catalytic Activity of Platinum Nanoparticles in Colloidal Solution. *Nano Lett.* **2004**, *4* (7), 1343–1348.
- (54) van Dorp, W.; Hagen, C.; Crozier, P.; Kruit, P. Growth Behavior Near the Ultimate Resolution of Nanometer-Scale Focused Electron Beam-Induced Deposition. *Nanotechnology* **2008**, *19* (22), 225305.
- (55) Shimojo, M.; Takeguchi, M.; Mitsuishi, K.; Tanaka, M.; Furuya, K. Formation of Nanoscale Platinum and Iron Oxide Structures Using Electron Beam Induced Deposition Techniques. *J. Phys.: Conf. Ser.* **2008**, *100*, 052016.
- (56) Schwalb, C. H.; Grimm, C.; Baranowski, M.; Sachser, R.; Porrati, F.; Reith, H.; Das, P.; Müller, J.; Völklein, F.; Kaya, A.; Huth,

- M. A Tunable Strain Sensor Using Nanogranular Metals. Sensors 2010, 10 (11), 9847-9856.
- (57) Moczała, M.; Kwoka, K.; Piasecki, T.; Kunicki, P.; Sierakowski, A.; Gotszalk, T. Fabrication and Characterization of Micromechanical Bridges with Strain Sensors Deposited Using Focused Electron Beam Induced Technology. *Microelectron. Eng.* **2017**, *176*, 111–115.
- (58) Kolb, F.; Schmoltner, K.; Huth, M.; Hohenau, A.; Krenn, J.; Klug, A.; List, E. J. W.; Plank, H. Variable Tunneling Barriers in FEBID Based PtC Metal-Matrix Nanocomposites as a Transducing Element for Humidity Sensing. *Nanotechnology* **2013**, *24* (30), 305501.
- (59) Wnuk, J. D.; Gorham, J. M.; Rosenberg, S. G.; van Dorp, W. F.; Madey, T. E.; Hagen, C. W.; Fairbrother, D. H. Electron Induced Surface Reactions of the Organometallic Precursor Trimethyl-(methylcyclopentadienyl)platinum(IV). *J. Phys. Chem. C* **2009**, *113* (6), 2487–2496.
- (60) Xue, Z.; Thridandam, H.; Kaesz, H. D.; Hicks, R. F. Organometallic Chemical Vapor Deposition of Platinum. Reaction Kinetics and Vapor Pressures of Precursors. *Chem. Mater.* **1992**, *4* (1), 162–166.
- (61) Botman, A.; Mulders, J.; Hagen, C. Creating Pure Nanostructures From Electron-Beam-Induced Deposition Using Purification Techniques: A Technology Perspective. *Nanotechnology* **2009**, *20* (37), 372001.
- (62) Villamor, E.; Casanova, F.; Trompenaars, P.; Mulders, J. Embedded Purification for Electron Beam Induced Pt Deposition Using MeCpPtMe₃. *Nanotechnology* **2015**, *26* (9), 095303.
- (63) Plank, H.; Noh, J. H.; Fowlkes, J. D.; Lester, K.; Lewis, B. B.; Rack, P. D. Electron-Beam-Assisted Oxygen Purification at Low Temperatures for Electron-Beam-Induced Pt Deposits: Towards Pure and High-Fidelity Nanostructures. ACS Appl. Mater. Interfaces 2014, 6 (2), 1018–1024.
- (64) Botman, A.; Mulders, J. J. L.; Weemaes, R.; Mentink, S. Purification of Platinum and Gold Structures after Electron-Beam-Induced Deposition. *Nanotechnology* **2006**, *17* (15), 3779–3785.
- (65) Geier, B.; Gspan, C.; Winkler, R.; Schmied, R.; Fowlkes, J. D.; Fitzek, H.; Rauch, S.; Rattenberger, J.; Rack, P. D.; Plank, H. Rapid and Highly Compact Purification for Focused Electron Beam Induced Deposits: A Low Temperature Approach Using Electron Stimulated H₂O Reactions. *J. Phys. Chem. C* **2014**, *118* (25), 14009–14016.
- (66) Warneke, Z.; Rohdenburg, M.; Warneke, J.; Kopyra, J.; Swiderek, P. Electron-driven and Thermal Chemistry During Water-Assisted Purification of Platinum Nanomaterials Generated by Electron Beam Induced Deposition. *Beilstein J. Nanotechnol.* **2018**, 9 (1), 77–90.
- (67) Frabboni, S.; Gazzadi, G.; Felisari, L.; Spessot, A. Fabrication by Electron Beam Induced Deposition and Transmission Electron Microscopic Characterization of Sub-10-nm Freestanding Pt Nanowires. *Appl. Phys. Lett.* **2006**, 88 (21), 213116.
- (68) Mehendale, S.; Mulders, J. J. L.; Trompenaars, P. H. F. A New Sequential EBID Process for the Creation of Pure Pt Structures from MeCpPtMe₃. *Nanotechnology* **2013**, *24*, 145303.
- (69) Hedhili, M. N.; Bredehoft, J. H.; Swiderek, P. Electron-Induced Reactions of MeCpPtMe₃ Investigated by HREELS. *J. Phys. Chem. C* **2009**, *113* (30), 13282–13286.
- (70) van Dorp, W. F.; Wnuk, J. D.; Gorham, J. M.; Fairbrother, D. H.; Madey, T. E.; Hagen, C. W. Electron Induced Dissociation of trimethyl(methylcyclopentadienyl)platinum(IV): Total Cross Section as a Function of Incident Electron Energy. *J. Appl. Phys.* **2009**, *106*, 074903.
- (71) Rosenberg, S. G.; Landheer, K.; Hagen, C. W.; Fairbrother, D. H. Substrate Temperature and Electron Fluence Effects on Metallic Films Created by Electron Beam Induced Deposition. *J. Vac. Sci. Technol., B: Nanotechnol. Microelectron.: Mater., Process., Meas., Phenom.* 2012, 30 (5), 051805.
- (72) Mulders, J. J. L.; Belova, L. M.; Riazanova, A. Electron Beam Induced Deposition at Elevated Temperatures: Compositional Changes and Purity Improvement. *Nanotechnology* **2011**, 22 (5), 055302.

- (73) Landheer, K.; Rosenberg, S.; Bernau, L.; Swiderek, P.; Utke, I.; Hagen, C.; Fairbrother, D. H. Low-Energy Electron-Induced Decomposition and Reactions of Adsorbed Tetrakis-(trifluorophosphine)platinum [Pt(PF₃)₄]. *J. Phys. Chem. C* **2011**, 115 (35), 17452–17463.
- (74) Ervin, M. H.; Chang, D.; Nichols, B.; Wickenden, A.; Barry, J.; Melngailis, J. Annealing of Electron Beam Induced Deposits of Platinum from Pt(PF₃)₄. J. Vac. Sci. Technol. B **2007**, 25, 2250–2254.
- (75) Spencer, J. A.; Brannaka, J. A.; Barclay, M.; McElwee-White, L.; Fairbrother, D. H. Electron-Induced Surface Reactions of η^3 -Allyl Ruthenium Tricarbonyl Bromide [$(\eta^3$ -C₃H₅)Ru(CO)₃Br]: Contrasting the Behavior of Different Ligands. *J. Phys. Chem. C* **2015**, *119* (27), 15349–15359.
- (76) Henderson, M. A.; Ramsier, R. D.; Yates, J. T. Low-energy Electron Induced Decomposition of Fe(CO)₅ Adsorbed on Ag(111). Surf. Sci. **1991**, 259, 173–182.
- (77) Spencer, J. A.; Barclay, M.; Gallagher, M. J.; Winkler, R.; Unlu, I.; Wu, Y. C.; Plank, H.; McElwee-White, L.; Fairbrother, D. H. Comparing Postdeposition Reactions of Electrons and Radicals with Pt Nanostructures Created by Focused Electron Beam Induced Deposition. *Beilstein J. Nanotechnol.* **2017**, *8*, 2410–2424.
- (78) De Teresa, J. M.; Córdoba, R.; Fernández-Pacheco, A.; Montero, O.; Strichovanec, P.; Ibarra, M. R. Origin of the Difference in the Resistivity of As-Grown Focused-Ion- and Focused-Electron-Beam-Induced Pt Nanodeposits. *J. Nanomater.* **2009**, 2009, 936863.
- (79) Belianinov, A.; Burch, M. J.; Ievlev, A.; Kim, S.; Stanford, M. G.; Mahady, K.; Lewis, B. B.; Fowlkes, J. D.; Rack, P. D.; Ovchinnikova, O. S. Direct Write of 3D Nanoscale Mesh Objects with Platinum Precursor via Focused Helium Ion Beam Induced Deposition. *Micromachines* **2020**, *11* (5), 527.
- (80) Salvador-Porroche, A.; Sangiao, S.; Philipp, P.; Cea, P.; Teresa, J. M. D. Optimization of Pt-C Deposits by Cryo-Fibid: Substantial Growth Rate Increase and Quasi-Metallic Behaviour. *Nanomaterials* **2020**, *10* (10), 1906.
- (81) Rohdenburg, M.; Winkler, R.; Kuhness, D.; Plank, H.; Swiderek, P. Water-Assisted Process for Purification of Ruthenium Nanomaterial Fabricated by Electron Beam Induced Deposition. ACS Appl. Nano. Mater. 2020, 3 (8), 8352–8364.
- (82) Rohdenburg, M.; Froch, J. E.; Martinovic, P.; Lobo, C. J.; Swiderek, P. Combined Ammonia and Electron Processing of a Carbon-Rich Ruthenium Nanomaterial Fabricated by Electron-Induced Deposition. *Micromachines* **2020**, *11* (8), 769.
- (83) Jurczyk, J.; Brewer, C. R.; Hawkins, O. M.; Polyakov, M. N.; Kapusta, C.; McElwee-White, L.; Utke, I. Focused electron beam induced deposition and post-growth purification using the heteroleptic Ru complex $(\eta^3-C_3H_5)$ Ru(CO)₃Br. ACS Appl. Mater. Interfaces **2019**, 11, 28164–28171.
- (84) Rohdenburg, M.; Martinović, P.; Ahlenhoff, K.; Koch, S.; Emmrich, D.; Gölzhäuser, A.; Swiderek, P. Cisplatin as a Potential Platinum Focused Electron Beam Induced Deposition Precursor: NH₃ Ligands Enhance the Electron-Induced Removal of Chlorine. *J. Phys. Chem. C* **2019**, *123* (35), 21774–21787.
- (85) Rohdenburg, M.; Boeckers, H.; Brewer, C. R.; McElwee-White, L.; Swiderek, P. Efficient NH₃-based Process to Remove Chlorine from Electron Beam Deposited Ruthenium Produced from $(\eta^3 C_3H_5)Ru(CO)_3Cl.$ Sci. Rep. **2020**, 10 (1), 10901.
- (86) Thorman, R. M.; Jensen, P. A.; Yu, J. C.; Matsuda, S. J.; McElwee-White, L.; Ingolfsson, O.; Fairbrother, D. H. Electron-Induced Reactions of Ru(CO)₄I₂: Gas Phase, Surface, and Electron Beam-Induced Deposition. *J. Phys. Chem. C* **2020**, *124* (19), 10593–10604.
- (87) Thorman, R. M.; Matsuda, S. J.; McElwee-White, L.; Fairbrother, D. H. Identifying and Rationalizing the Differing Surface Reactions of Low-Energy Electrons and Ions with an Organometallic Precursor. J. Phys. Chem. Lett. 2020, 11 (6), 2006–2013.
- (88) Bilgilisoy, E.; Thorman, R. M.; Yu, J.-C.; Dunn, T. B.; Marbach, H.; McElwee-White, L.; Fairbrother, D. H. Surface Reactions of Low-Energy Argon Ions with Organometallic Precursors. *J. Phys. Chem. C* **2020**, *124*, 24795–24808.

- (89) El-Sayed, M. A. Small Is Different: Shape-, Size-, and Composition-Dependent Properties of Some Colloidal Semiconductor Nanocrystals. *Acc. Chem. Res.* **2004**, *37* (5), 326–333.
- (90) Jain, P. K.; Lee, K. S.; El-Sayed, I. H.; El-Sayed, M. A. Calculated Absorption and Scattering Properties of Gold Nanoparticles of Different Size, Shape, and Composition: Applications in Biological Imaging and Biomedicine. *J. Phys. Chem. B* **2006**, *110* (14), 7238–7248.
- (91) Naik, G. V.; Shalaev, V. M.; Boltasseva, A. Alternative Plasmonic Materials: Beyond Gold and Silver. *Adv. Mater.* **2013**, 25 (24), 3264–3294.
- (92) Liu, Z.; Zhou, C.; Zheng, B.; Qian, L.; Mo, Y.; Luo, F.; Shi, Y.; Choi, M. M. F.; Xiao, D. In situ Synthesis of Gold Nanoparticles on Porous Polyacrylonitrile Nanofibers for Sensing Applications. *Analyst* **2011**, *136* (21), 4545–4551.
- (93) Qin, L.; Zeng, G.; Lai, C.; Huang, D.; Xu, P.; Zhang, C.; Cheng, M.; Liu, X.; Liu, S.; Li, B.; Yi, H. "Gold Rush" in Modern Science: Fabrication Strategies and Typical Advanced Applications of Gold Nanoparticles In Sensing. *Coord. Chem. Rev.* **2018**, *359*, 1–31.
- (94) Weissleder, R. A Clearer Vision for In Vivo Imaging. *Nat. Biotechnol.* **2001**, *19* (4), 316–317.
- (95) Wu, Y.; Ali, M. R. K.; Chen, K.; Fang, N.; El-Sayed, M. A. Gold Nanoparticles in Biological Optical Imaging. *Nano Today* **2019**, *24*, 120–140.
- (96) Link, S.; El-Sayed, M. A. Shape and size Dependence of Radiative, Non-Radiative and Photothermal Properties of Gold Nanocrystals. *Int. Rev. Phys. Chem.* **2000**, *19* (3), 409–453.
- (97) Sharifi, M.; Attar, F.; Saboury, A. A.; Akhtari, K.; Hooshmand, N.; Hasan, A.; El-Sayed, M. A.; Falahati, M. Plasmonic Gold Nanoparticles: Optical Manipulation, Imaging, Drug Delivery and Therapy. *J. Controlled Release* **2019**, 311–312, 170–189.
- (98) Huang, X.; El-Sayed, I. H.; Qian, W.; El-Sayed, M. A. Cancer Cell Imaging and Photothermal Therapy in the Near-Infrared Region by Using Gold Nanorods. *J. Am. Chem. Soc.* **2006**, 128 (6), 2115–2120.
- (99) Huang, X.; El-Sayed, M. A. Gold Nanoparticles: Optical Properties and Implementations in Cancer Diagnosis and Photothermal Therapy. *J. Adv. Res.* **2010**, *1* (1), 13–28.
- (100) Puydinger Dos Santos, M. V.; Szkudlarek, A.; Rydosz, A.; Guerra-Nunez, C.; Beron, F.; Pirota, K. R.; Moshkalev, S.; Diniz, J. A.; Utke, I. Comparative Study of Post-Growth Annealing of Cu(hfac)₂, Co₂(CO)₈ and Me₂Au(acac) Metal Precursors Deposited by FEBID. *Beilstein J. Nanotechnol.* **2018**, *9*, 91–101.
- (101) Winkler, R.; Schmidt, F. P.; Haselmann, U.; Fowlkes, J. D.; Lewis, B. B.; Kothleitner, G.; Rack, P. D.; Plank, H. Direct-Write 3D Nanoprinting of Plasmonic Structures. *ACS Appl. Mater. Interfaces* **2017**, 9 (9), 8233–8240.
- (102) van Dorp, W. F.; Wu, X.; Mulders, J. J. L.; Harder, S.; Rudolf, P.; De Hosson, J. T. M. Gold Complexes for Focused Electron Beam Induced Deposition. *Langmuir* **2014**, *30*, 12097.
- (103) Shawrav, M. M.; Taus, P.; Wanzenboeck, H. D.; Schinnerl, M.; Stoger-Pollach, M.; Schwarz, S.; Steiger-Thirsfeld, A.; Bertagnolli, E. Highly Conductive and Pure Gold Nanostructures Grown by Electron Beam Induced Deposition. *Sci. Rep.* **2016**, *6*, 34003.
- (104) Folch, A.; Servat, J.; Esteve, J.; Tejada, J.; Seco, M. Highvacuum Versus "Environmental" Electron Beam Deposition. *J. Vac. Sci. Technol., B: Microelectron. Process. Phenom.* **1996**, 14 (4), 2609–2614.
- (105) Utke, I.; Jenke, M. G.; Roling, C.; Thiesen, P. H.; Iakovlev, V.; Sirbu, A.; Mereuta, A.; Caliman, A.; Kapon, E. Polarisation Stabilisation of Vertical Cavity Surface Emitting Lasers by Minimally Invasive Focused Electron Beam Triggered Chemistry. *Nanoscale* **2011**, 3 (7), 2718–2722.
- (106) Wnuk, J. D.; Gorham, J. M.; Rosenberg, S. G.; van Dorp, W. F.; Madey, T. E.; Hagen, C. W.; Fairbrother, D. H. Electron Beam Irradiation of dimethyl(acetylacetonate) gold(III) Adsorbed Onto Solid Substrates. *J. Appl. Phys.* **2010**, *107* (5), 054301.
- (107) Belic, D.; Shawrav, M. M.; Bertagnolli, E.; Wanzenboeck, H. D. Direct Writing of Gold Nanostructures with an Electron Beam: On

- the way to Pure Nanostructures by Combining Optimized Deposition with Oxygen-Plasma Treatment. *Beilstein J. Nanotechnol.* **2017**, 8, 2530–2543.
- (108) Brintlinger, T.; Fuhrer, M. S.; Melngailis, J.; Utke, I.; Bret, T.; Perentes, A.; Hoffmann, P.; Abourida, M.; Doppelt, P. Electrodes for Carbon Nanotube Devices by Focused Electron Beam Induced Deposition of Gold. J. Vac. Sci. Technol., B: Microelectron. Process. Phenom. 2005, 23 (6), 3174–3177.
- (109) Hoffmann, P.; Utke, I.; Cicoira, F.; Dwir, B.; Leifer, K.; Kapon, E.; Doppelt, P. Focused Electron Beam Induced Deposition of Gold and Rhodium. MRS Online Proceedings Library 2000, 624 (1), 171–177.
- (110) Berseth, C. A.; Dwir, B.; Utke, I.; Pier, H.; Rudra, A.; Iakovlev, V. P.; Kapon, E.; Moser, M. Vertical Cavity Surface Emitting Lasers Incorporating Structured Mirrors Patterned by Electron-Beam Lithography. J. Vac. Sci. Technol., B: Microelectron. Process. Phenom. 1999, 17 (6), 3222–3225.
- (111) Mulders, J. J. L.; Veerhoek, J. M.; Bosch, E. G. T.; Trompenaars, P. H. F. Fabrication of Pure Gold Nanostructures by Electron Beam Induced Deposition with Au(CO)Cl Precursor: Deposition Characteristics and Primary Beam Scattering Effects. J. Phys. D: Appl. Phys. 2012, 45 (47), 475301.
- (112) Utke, I.; Hoffmann, P.; Dwir, B.; Leifer, K.; Kapon, E.; Doppelt, P. Focused Electron Beam Induced Deposition of Gold. *J. Vac. Sci. Technol., B: Microelectron. Process. Phenom.* **2000**, *18* (6), 3168–3171.
- (113) Carden, W. G.; Thorman, R. M.; Unlu, I.; Abboud, K. A.; Fairbrother, D. H.; McElwee-White, L. Design, Synthesis, and Evaluation of CF₃AuCNR Precursors for Focused Electron Beam-Induced Deposition of Gold. ACS Appl. Mater. Interfaces 2019, 11, 11976–11987.
- (114) Stockman, M. I.; Kneipp, K.; Bozhevolnyi, S. I.; Saha, S.; Dutta, A.; Ndukaife, J.; Kinsey, N.; Reddy, H.; Guler, U.; Shalaev, V. M.; Boltasseva, A.; Gholipour, B.; Krishnamoorthy, H. N. S.; MacDonald, K. F.; Soci, C.; Zheludev, N. I.; Savinov, V.; Singh, R.; Groß, P.; Lienau, C.; Vadai, M.; Solomon, M. L.; Barton, D. R.; Lawrence, M.; Dionne, J. A.; Boriskina, S. V.; Esteban, R.; Aizpurua, J.; Zhang, X.; Yang, S.; Wang, D.; Wang, W.; Odom, T. W.; Accanto, N.; de Roque, P. M.; Hancu, I. M.; Piatkowski, L.; van Hulst, N. F.; Kling, M. F. Roadmap on Plasmonics. J. Opt. 2018, 20 (4), 043001. (115) Spencer, J. A.; Carden, W. G.; McElwee-White, L.; Fairbrother, D. H. Unpublished results.
- (116) Glessi, C.; Mahgoub, A.; Hagen, C. W.; Tilset, M. Gold(I) N-heterocyclic Carbene Precursors for Focused Electron Beam-Induced Deposition. *Beilstein J. Nanotechnol.* **2021**, *12*, 257–269.
- (117) Dubner, A. D.; Wagner, A.; Melngailis, J.; Thompson, C. V. The Role of the Ion-Solid Interaction in Ion-Beam-Induced Deposition of Gold. *J. Appl. Phys.* **1991**, 70 (2), 665–673.
- (118) Ro, J.; Thompson, C.; Melngailis, J. Mechanism of Ion Beam Induced Deposition of Gold. J. Vac. Sci. Technol., B: Microelectron. Process. Phenom. 1994, 12 (1), 73–77.
- (119) Shedd, G. M.; Lezec, H.; Dubner, A. D.; Melngailis, J. Focused Ion Beam Induced Deposition of Gold. *Appl. Phys. Lett.* **1986**, 49 (23), 1584–1586.
- (120) Joy, D. C. Helium Ion Microscopy: Principles and Applications; Springer-Verlag: New York, 2013.
- (121) Funsten, H. O.; Boring, J. W.; Johnson, R. E.; Brown, W. L. Low-temperature beam-induced deposition of thin tin films. *J. Appl. Phys.* **1992**, *71* (3), 1475–1484.
- (122) Porrati, F.; Sachser, R.; Gazzadi, G. C.; Frabboni, S.; Huth, M. Fabrication of FeSi and Fe₃Si Compounds by Electron Beam Induced Mixing of [Fe/Si]₂ and [Fe₃/Si]₂ Multilayers Grown by Focused Electron Beam Induced Deposition. *J. Appl. Phys.* **2016**, *119* (23), 234306.
- (123) Porrati, F.; Pohlit, M.; Müller, J.; Barth, S.; Biegger, F.; Gspan, C.; Plank, H.; Huth, M. Direct Writing of CoFe Alloy Nanostructures by Focused Electron Beam Induced Deposition from a Heteronuclear Precursor. *Nanotechnology* **2015**, *26* (47), 475701.

- (124) Puydinger dos Santos, M. V.; Barth, S.; Béron, F.; Pirota, K. R.; Pinto, A. L.; Sinnecker, J. P.; Moshkalev, S.; Diniz, J. A.; Utke, I. Magnetoelectrical Transport Improvements of Postgrowth Annealed Iron—Cobalt Nanocomposites: A Possible Route for Future Room-Temperature Spintronics. ACS Appl. Nano. Mater. 2018, 1 (7), 3364—3374.
- (125) Che, R. C.; Takeguchi, M.; Shimojo, M.; Zhang, W.; Furuya, K. Fabrication and Electron Holography Characterization of FePt Alloy Nanorods. *Appl. Phys. Lett.* **2005**, 87 (22), 223109.
- (126) Kumar T P, R.; Unlu, I.; Barth, S.; Ingólfsson, O.; Fairbrother, D. H. Electron Induced Surface Reactions of HFeCo₃(CO)₁₂, a Bimetallic Precursor for Focused Electron Beam Induced Deposition (FEBID). *J. Phys. Chem. C* **2018**, *122* (5), 2648–2660.
- (127) Unlu, I.; Spencer, J.; Johnson, K. R.; Thorman, R.; Ingólfsson, O.; McElwee-White, L.; Fairbrother, D. H. Electron Induced Surface Reactions of $(\eta^5\text{-}C_5H_5)\text{Fe}(\text{CO})_2\text{Mn}(\text{CO})_5$, a Potential Heterobimetallic Precursor for Focused Electron Beam Induced Deposition (FEBID). *Phys. Chem. Chem. Phys.* **2018**, 20 (11), 7862–7874.